

Exploring the planetary-mass population in the Upper Scorpius association [★]

N. Lodieu ^{1,2}†, N. C. Hambly ³, N. J. G. Cross ³

¹*Instituto de Astrofísica de Canarias (IAC), C/ Vía Láctea s/n, E-38200 La Laguna, Tenerife, Spain*

²*Departamento de Astrofísica, Universidad de La Laguna (ULL), E-38206 La Laguna, Tenerife, Spain*

³*Scottish Universities Physics Alliance (SUPA), Institute for Astronomy, School of Physics and Astronomy, University of Edinburgh, Royal Observatory, Blackford Hill, Edinburgh EH9 3HJ, UK*

Accepted 1 March 2021. Received 1 March 2021; in original form 1 March 2021

ABSTRACT

We aim at identifying very low-mass isolated planetary-mass member candidates in the nearest OB association to the Sun, Upper Scorpius (145 pc; 5–10 Myr), to constrain the form and shape of the luminosity function and mass spectrum in this regime. We conducted a deep multi-band ($Y = 21.2$, $J = 20.5$, $Z = 22.0$ mag) photometric survey of six square degrees in the central region of Upper Scorpius. We extend the current sequence of astrometric and spectroscopic members by about two magnitudes in Y and one magnitude in J , reaching potentially T-type free-floating members in the association with predicted masses below 5 Jupiter masses, well into the planetary-mass regime. We extracted a sample of 57 candidates in this area and present infrared spectroscopy confirming two of them as young L-type members with characteristic spectral features of 10 Myr-old brown dwarfs. Among the 57 candidates, we highlight 10 new candidates fainter than the coolest members previously confirmed spectroscopically. We do not see any obvious sign of decrease in the mass spectrum of the association, suggesting that star processes can form substellar objects with masses down to 4–5 Jupiter masses.

Key words: Stars: low-mass stars and brown dwarfs — techniques: photometric, spectroscopic — surveys — stars: luminosity function, mass function

1 INTRODUCTION

The existence of brown dwarfs and exoplanets is now well established with several hundreds of examples discovered over the past 25 years (Mayor & Queloz 1995; Rebolo et al. 1995; Nakajima et al. 1995). Large-scale surveys for field ultracool dwarfs and deep pencil-beam surveys of specific regions have now identified substellar objects down to a few Jupiter masses with properties differing depending on their age, environment or metallicity. The shape of the substellar present-day mass function (Salpeter 1955; Miller & Scalo 1979; Scalo 1986) in the solar neighbourhood seems to indicate a power law index α of 0.6, where $dN/dM \propto M^{-\alpha}$ accounting for all members of the 20 pc sample (Kirkpatrick et al. 2019). This slope is consistent with the substellar shape of the mass functions in star-forming regions (review by Bastian et al. 2010), nearby moving groups (Liu et al. 2013; Gagné et al. 2015b; Faherty et al. 2016), and young clusters (review by Luhman 2012). How massive can the least massive fragment that star formation mechanisms can form (also referred to as the limit of fragmentation), remains an open question. Early estimates suggested 7 Jupiter masses (hereafter M_{Jup}) (Low & Lynden-Bell 1976; Rees 1976; Silk 1977) but this limit may change when including rotation or magnetic fields in the simulations (Boss

1988; Boyd & Whitworth 2005; Whitworth & Stamatellos 2006; Boley & Durisen 2010; Kratter et al. 2010; Forgan & Rice 2011; Rogers & Wadsley 2012). From the aforementioned studies of nearby substellar objects in the solar vicinity and in young regions, the limit seems to be consistently below 5 M_{Jup} .

Upper Scorpius (USco) is part of the nearest OB association to the Sun, Scorpius Centaurus. The region is located at 145 pc from the Sun (de Bruijne et al. 1997) and has an age of 5–10 Myr (Preibisch & Zinnecker 1999; Preibisch et al. 2001; Pecaut et al. 2012; Song et al. 2012; David et al. 2019). USco members show a significant mean proper motion compared to stars along its line of sight (mean value of -11 and -25 mas/yr in right ascension and declination, respectively; de Bruijne et al. 1997; de Zeeuw et al. 1999). The high-mass population of USco has been explored in X-rays (Walter et al. 1994; Kunkel 1999; Preibisch et al. 1998), astrometrically (de Bruijne et al. 1997; de Zeeuw et al. 1999; Cook et al. 2017; Luhman & Esplin 2020a) in the optical (Ardila et al. 2000; Martín et al. 2004; Slesnick et al. 2006, 2008), and in the infrared (Lodieu et al. 2006, 2007a; Kraus et al. 2008; Béjar et al. 2008; Lafrenière et al. 2010; Dawson et al. 2011; Lodieu et al. 2011a; Lafrenière et al. 2011; Dawson et al. 2013; Lodieu 2013; Lafrenière et al. 2014; Dawson et al. 2014; Best et al. 2017). Low-mass stars and brown dwarfs in USco have been subject to numerous studies over the past years thanks to the arrival of wide and deep surveys (Preibisch et al. 2001; Preibisch & Zinnecker 2002; Lodieu et al. 2007a, 2011b; Peña Ramírez et al. 2016), and more recently the *Gaia* mission (Gaia Collaboration et al. 2018), yielding a relatively well-defined mass

[★] Based on observations collected at the European Organisation for Astronomical Research in the Southern Hemisphere under ESO programmes 089-C.0102(ABC), 097.C-0781(A), and 0101.C-0565.

† E-mail: nlodieu@iac.es

function below the stellar/substellar limit in this region (Luhman & Esplin 2020a). The Kepler K2 mission (Borucki et al. 2010; Lissauer et al. 2014; Batalha 2014) has revealed the first eclipsing binaries in USco over a wide range of masses, giving the first independent mass and radius determinations at 5–10 Myr (Alonso et al. 2015; Kraus et al. 2015; Lodieu et al. 2015; David et al. 2016b, 2019) as well as the first Neptune-size planet orbiting a M3 star (Mann et al. 2016; David et al. 2016a).

Lodieu et al. (2018a) recently identified the first L dwarf sequence in USco with optical and infrared spectroscopic characterisation. These authors identified L-type candidates in a deep *ZYJ* survey (Lodieu et al. 2013b) conducted with the Visible Infrared Survey Telescope (VISTA; Emerson 2001; Dalton et al. 2006). In this paper we release a new, *Y*-band survey 2 magnitudes deeper over half of the area compared to the former survey to look for isolated planetary-mass candidates with ages of 5–10 Myr and investigate the shape of the luminosity and mass function below the deuterium-burning limit. In Section 2 we present the deep infrared observations obtained with European Southern Observatory (ESO) VISTA/VIRCAM located in Paranal (Chile) and the data reduction methods. In Section 3 we detail the Sloan *z*-band survey conducted with the Hyper Suprime-Cam camera on Subaru in Mauna Kea (Hawaii, USA). In Section 4 we describe the selection of potential planetary-mass member candidates of the USco association. In Section 6 we discuss the nature of our candidates and the implications on the shape of the IMF and the theory of the fragmentation limit.

2 THE VISTA DEEP SURVEYS

This study makes use of two different but complementary VISTA surveys described below. VISTA is a 4-m telescope (Emerson 2001; Emerson et al. 2004) based in Paranal (Chile) and equipped with the VISTA InfraRed CAMera (VIRCAM; Dalton et al. 2006). VIRCAM is fitted with 16 infrared detectors with pixels of 0.339 arcsec offering a field of view of 1.65 square degrees.

2.1 VISTA/VIRCAM observations

On the one hand, we re-processed the deep VISTA *ZYJ* survey described in Lodieu et al. (2013b) to extract PSF photometry instead of aperture photometry for optimal completeness and best accuracy for faint point sources in these relatively crowded fields. To summarise, these surveys cover 13.5 square degrees towards the central region of USco. The observations took place between April and May 2012 down to 100% completeness limits of $Z = 22.0$ mag, $Y = 21.2$ mag, and $J = 20.5$ mag, respectively. We refer the reader to Lodieu et al. (2013b) for more details. We will refer to that survey as the ‘first epoch’ throughout the paper. This work identified tens of brown dwarf and planetary-mass members, 12 of them being confirmed spectroscopically as 5–10 Myr-old L1–L7 members (Lodieu et al. 2018a) with an independent classification by Luhman et al. (2018).

On the other hand, we conducted a deeper *Y*-band survey with VISTA/VIRCAM to be sensitive to fainter and cooler USco members because the first epoch was limited in depth by the *Y* and *Z* filters. We observed four VISTA/VIRCAM tiles in the *Y*-band filter (centered at 1.02 ± 0.10 micron) between May and July 2016 as part of ESO program 095.C-0781(A) (PI Lodieu). We gather the logs of observations in Table 1 compiling seeing, airmass, and ellipticity information for each tile. We set the on-source integrations to 60 s repeated twice with six paw-print positions and five jitter positions, resulting in a 1h total on-source integration for each tile. We repeated

this observing block seven times during the May–July 2016 period for the four tiles to achieve a 100% completeness limit of $Y = 22.6$ mag over 6.6 square degrees. Due to the differences in the tiling configurations automatically processed by the ESO survey definition tool, the common area between the two VISTA survey is about six square degrees (Fig. 1).

2.2 Point Spread Function (PSF) Photometry

VISTA Science Archive (VSA; Cross et al. 2012) standard pipeline products consist of instrumentally corrected images combined into stacks and source catalogue extraction with fixed apertures from those images. While the fixed-aperture source extraction (Irwin et al. 2004) is optimised for faint point sources, the detection and deblending of faint stars, in particular those near to much brighter objects, is not optimal. Our deepest stacked images are rather more crowded than the shallow and wide survey images for which the aperture source extraction has been optimised, so we employed Point Spread Function (PSF) fitted photometry in creating our source detection lists from the VSA image products (see for example Mauro et al. 2013).

We employed DAOPHOT (Stetson 1987) in a recent incarnation running within the IRAF/PyRAF environment (Tody 1986, 1993; Davis 1999; Greenfield & White 2006; Science Software Branch at STScI 2012). We followed standard best-practice in detecting sources, defining the PSF and then using that PSF to fit all detected objects, simultaneously within small groups, to extract source positions and fluxes. Matched-filter source detection at a 2.8σ threshold was run on all the images using the DAOFIND task. A selection of 100 PSF stars was made for each image automatically from the DAOFIND output, where every PSF star was required to have a magnitude between 3.0 and 3.5 above the detection limit (i.e. intermediate in brightness for good signal-to-noise but not so bright as to be affected by non-linearity or saturation), and having no other detected source within two PSF fitting radii. Additionally we required our PSF stars to have values of the DAOFIND shape parameters SHARP, SROUND and GROUND within 1σ of their median values in order to restrict the selection to faint, point-like images in every case. The PSF model in DAOPHOT consists of an underlying analytical function with additional residual corrections (Stetson 1987). In order to choose the most appropriate analytical model amongst the available options, we made trial fits and compared the residual profile scatter for all. We finally settled on the ‘penny2’ option (a Gaussian core with Lorentzian wings, both of which are elliptical, and tilted arbitrarily and independently to the image coordinate axes). In order to account for position-dependent variation in the PSF we selected ‘varorder’ equal to 2 for quadratically varying terms in the residual correction look-up tables of the combined PSF model. A default PSF model radius of 11 pixels was employed during PSF modelling, while a PSF fitting radius of twice the full-width-half-maximum (FWHM) measured in each image was employed at the PSF photometry stage when photometry all detected sources.

We matched the *Y* and *J* catalogues within a conservative radius of 3 arcsec, yielding a total of 887,175 sources. We applied two quality criteria on the sharpness (between -0.5 and 0.5) and χ^2 (less than 3.0) parameters in both filters that returned 617,715 objects, which will be our input catalogue in the rest of our analysis. We note that the number of sources with pairing radii larger than 1 arcsec is relative constant. We count 7106 pairs beyond 1 arcsec, resulting in a contamination less than 1.2%. We show the resulting ($Y - J, J$) colour-magnitude diagram in the left-hand side of Fig. 2. In the right-hand side of Fig. 2, we plot the same diagram and overplot known USco members from the literature and our photometric candidates.

Table 1. Logs of the VISTA/VIRCAM Y -band observations. We list the name of the tiles with their coordinates in sexagesimal format, the range of date+time of observations, the total on-source exposure time, the median seeing, mean ellipticity, and airmass at the time of observations. We give the average parameters for each stacked tile made of seven individual tiles combined together.

Tile	R.A.	Dec	Date_min	Date_max	ExpT	Seeing	Ell	Airmass
	hh:mm:ss.ss	°:′:″	yyyy-mm-dd	yyyy-mm-dd	seconds	arcsec		
tile112	243.2118900	−23.0915800	2016-05-19 06:25:08.3	2016-07-12 23:17:48.2	8200	1.04	0.05	1.16
tile111	241.6261650	−23.0908100	2016-05-18 02:54:48.4	2016-06-29 23:57:34.6	8200	0.92	0.05	1.18
tile122	243.2064900	−21.9993800	2016-06-01 06:01:13.2	2016-07-11 23:31:25.3	8200	1.03	0.05	1.13
tile121	241.6331400	−21.9986100	2016-06-01 04:49:03.2	2016-06-30 05:00:20.3	8200	1.03	0.05	1.13

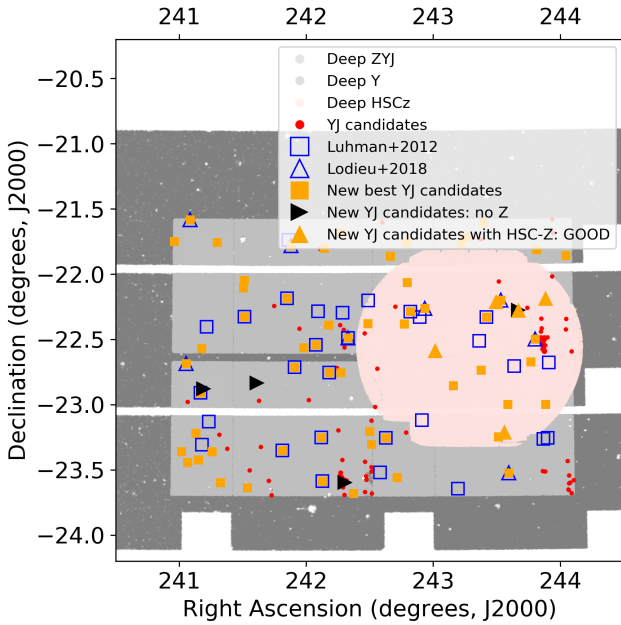


Figure 1. Location of the four deep Y -band tiles (light grey) on top of the nine first epoch observations conducted in ZYJ (grey) with VISTA (Lodieu et al. 2013b). Overplotted is the coverage of the deep Subaru HSC survey (light rose). Known members from Luhman & Mamajek (2012) and Lodieu et al. (2018a) are shown as blue open squares and triangles, respectively. The new candidates selected in this work are highlighted as black and orange symbols.

We cross-matched the Y, J catalogue with photometry from our previous VISTA Z -band as well as $H + K$ from the UKIRT Infrared Deep Sky Survey (UKIDSS; Lawrence et al. 2007) Galactic Clusters Survey (GCS) Data Release 9 (DR9), the AllWISE survey (Cutri et al. 2013; Cutri & et al. 2014), and the Panoramic Survey Telescope and Rapid Response System catalogue (Pan-STARRS; Chambers et al. 2016) with a pairing radius of 3 arcsec in each case. We will make the full catalogue available to the community via VizieR at the Centre de Données de Strasbourg. The full table contains the coordinates in J2000, the magnitudes in each filter with their associated uncertainties, the sharpness and χ^2 parameters given by daophot and allstar in IRAF, the proper motion in mas, and the cross-match with other catalogues like the UKIDSS GCS DR9, AllWISE, and PanStarrs DR1.

3 THE HYPER SUPRIME-CAM SURVEY

3.1 Subaru Hyper Suprime-Cam observations

The Hyper Suprime-Cam (HSC) is a very large charge-coupled detector (CCD) mosaic camera mounted at prime focus of the Subaru 8.2-m Telescope (Iye et al. 2004) in Mauna Kea, Hawaii. The HSC uses 104 science charge-coupled devices sensitive to optical wavelengths, offering a 1.5-degree field-of-view in diameter with a pixel size of 0.17 arcsec (Miyazaki et al. 2018; Komiyama et al. 2018; Kawanomoto et al. 2018; Furusawa et al. 2018). The auto-guiding is ensured with four CCDs while the focus is monitored with eight CCDs. We employed the Sloan z -band filter centered at 8921.66 Å with a width of 792.99 Å to be as sensitive as possible to the coolest members of the association, with the goal of improving on the depth of the deep Z survey (Section 2.1).

The observations were collected in service mode on 25 May 2020 between UT = 10h58 and 12h40 as part of programme S20A-QN098 (PI Lodieu). The airmass of USco from Mauna Kea was between 1.4 and 1.8. The seeing was better than 0.8 arcsec. The transparency was higher than 90% and the sky was dark with no moon. We collected four blocks of six integrations of 252 seconds, yielding a total exposure of 5040s on a single 1.5-degree field centered at RA = 16h13m, dec = 22°36′ (Fig. 1).

3.2 Data reduction and catalogue generation

A standard data reduction procedure was employed in processing the HSC via the LSST pipeline stack (Jenness & LSST Data Management Team 2017). Instrumental correction consisted of bias pre-subtraction, dark, illumination and flat corrections along with a default brighter-fatter kernel correction (Bosch et al. 2018). Single-visit processing to create accurate astrometric and photometric calibration at the individual CCD level was performed with respect to the PanSTARRS DR1 catalogue (Chambers et al. 2016). The 20 individual frames from each of the 104 CCDs available within the field visit were warped and stacked in patches to create a deep stack image from which sources were extracted and measured for point-spread function (PSF) fitted photometry, again using the standard LSST routines. The HSC- Z band photometry, by default on an AB magnitude scale, was transformed to the VIRCAM Vega system using a correction $z_{\text{Vega}} = z_{\text{AB}} - 0.521$ (Cross et al. 2012). Finally, a small ± 0.05 linear colour correction was applied to the photometry as a function of $z - J$ colour to put the HSC- Z measurements on the natural VIRCAM Z photometric system.

We extracted a total 853,676 sources with a completeness limit of $Z = 24.3$ mag, reduced to 379,279 objects when removing saturated sources (typically brighter than 17.5 mag), and extended sources as

well as those with poor PSF fitting. We cross-matched the full deep *ZYJ* VISTA catalogue with the good-quality sources in the HSC catalogue and found 162,735 objects in common. We will make this full VISTA+Subaru catalogue of identifiers, coordinates, *Z* photometry with its associated error, classification (point source or extended), and flag available to the community via VizieR.

4 IDENTIFICATION OF FAINT USCO MEMBER CANDIDATES

The goal of this section is to focus on member candidates fainter than the coolest L dwarfs identified in our original *ZYJ* survey (Lodieu et al. 2013b) and recently confirmed spectroscopically (Lodieu et al. 2018a) by combining the deep *Y*-band second epoch survey with the first epoch *ZYJ* survey. To set the scene, the two L7 spectroscopic members have $Y = 20.8\text{--}21.0$ mag, $J \sim 19.3$ mag, and *Z* magnitudes beyond the 100% completeness limit of the first epoch ($Z = 22$ mag). We start by reviewing our current knowledge on the photometric properties of field and young L and T dwarfs before jumping into the selection of USco brown dwarfs and isolated planetary-mass objects.

We emphasise that studies of isolated planetary-mass objects of T-type in clusters and star-forming regions younger than 20 Myr currently are rather limited. Most objects are candidates whose membership remains under debate or that need to be confirmed through spectroscopy and/or astrometry (e.g. Burgess et al. 2009; Haisch et al. 2010; Peña Ramírez et al. 2011; Barsony et al. 2012; Spezzi et al. 2012; Scholz et al. 2012; Lodieu et al. 2013a; Chiang & Chen 2015; Peña Ramírez et al. 2015).

4.1 Photometric properties of field L/T dwarfs

We looked at the colours and absolute magnitudes of field L and T dwarfs (Dupuy & Liu 2012) and located them in several diagrams (see figures in this paper) to guide the identification of their younger counterparts. We draw the following conclusions, keeping in mind that our current poor knowledge of the spectral energy distribution of T-type objects at young ages.

- The $Y - J$ colours of field L/T dwarfs are approximately constant around 1 mag, going from 1.2 mag for L6 to 1.1 mag for T8 but with values slightly below 1.0 mag for T2 and T3 types (Dupuy & Liu 2012). From the synthetic colours of L/T dwarfs (Hewett et al. 2006), a kink towards the blue is observed in the $Y - J$ colours for transition sources followed by a relatively constant value from mid-T dwarfs (right-hand side panel in Fig. 2).

- The $Z - J$ vs $Y - J$ diagram indicates that L/T transition objects have $Z - J$ colours as blue as 2.5 mag (Hewett et al. 2006) with a larger dispersion for L/T transition dwarfs and an average $Z - J$ colour that keeps being redder with later spectral types (Fig. 3).

- The $Z - K$ colours of L/T transition objects show a similar dispersion as in $Z - J$ while their $J - K$ colours become bluer from T0 ($J - K = 1.4$ mag) to T1 ($J - K = 1.13$ mag) as seen in the right panel in Fig. 4.

- The absolute *Y* magnitude of a T4 is as bright as a L7 but slightly fainter than a L6.

- A old field T4 dwarf has $SDSS_z \sim 23.8$ mag (Hewett et al. 2006; Schmidt et al. 2010) and $Y, J = 21.13, 20.13$ mag (Dupuy & Liu 2012) but USco members tend to be 1 mag brighter than field objects.

4.2 Photometric properties of young L/T dwarfs

We examined the colours of five red young L7 dwarfs within 50 pc with ages less than 20 Myr (determined via membership of young moving groups) similar to USco recently published in the literature (e.g. Looper et al. 2007; Gauza et al. 2015; Gagné et al. 2015a; Filippazzo et al. 2015; Faherty et al. 2016; Liu et al. 2016; Schneider et al. 2016). We also compiled three T dwarfs with older ages but well-constrained ages based on their high-probability membership of the AB Dor (GUPSc b (T3.5), SDSS J11101001+0116130 (T5.5); 70–130 Myr; Gagné et al. 2017a) and Carina-Near (SIMP01365662+0933473 (T2.5); 150–300 Myr; Gagné et al. 2017b) young moving groups plotted as blue filled symbols in all colour-magnitude diagrams of this manuscript. Unfortunately, there are no *Z* magnitudes published for these sources, which appears as a key filter in our study. We also added to the diagrams three L/T transition member candidates (blue squares) of the Pleiades (Zapatero Osorio et al. 2014b) at an age of 125 Myr (Stauffer et al. 1998) identified in a deep photometric survey with astrometric information (Zapatero Osorio et al. 2014a). We plot all these young L/T transition sources with $Y, J, w1, w2$ photometry compiled from the literature in the diagrams presented in this manuscript after correcting their apparent magnitudes for their distances and applying the distance modulus of the USco association (145 pc; Luhman & Esplin 2020b). We note that all five young L7 dwarfs are intrinsically fainter than the USco L7 members. They show bluer $Y - J$ colours but redder colours in other combinations of filters that may come from differences in the optical thickness of the dust cloud deck (Marocco et al. 2014).

4.3 YJ photometric candidates

As a first step, we carefully looked at the $(Y - J, Y)$ diagram in the left-hand side panel in Fig. 2. We suggest that the USco sequence is visible, running from around $(Y - J, Y) = (0.75, 15.0)$ to $(1.45, 20.0)$ to $(2.6, 22.5)$, with the reddest candidate at around $(3.1, 22.7)$. The first part of the USco sequence down to $Y = 20$ mag is supported by known members while the bottom part is based on the morphology of the colour-magnitude diagram. To confirm this hypothesis, we overplot on this diagram known USco members from Luhman & Mamajek (2012) and spectroscopic L dwarf members (Lodieu et al. 2018a), displayed as open blue squares and triangles in Fig. 2, respectively. Hence, we designed a series of selection lines following the USco sequence but shifted to the blue of the sequence to be conservative. We limited our search to sources fainter than $Y = 15$ mag because brighter sources tend to be saturated in our deep survey. Moreover, our goal is to identify the coolest L and T-type members and this region has been well surveyed at brighter magnitudes by various teams (e.g. Lodieu et al. 2007a; Dawson et al. 2011; Lodieu et al. 2011a; Luhman & Mamajek 2012; Dawson et al. 2013; Best et al. 2017). This selection returned 157 candidates and is abbreviated below as “New cand YJ ” (red dots in all figures). Among these 157, 21 and 16 have matching radii larger than 1.0 and 1.5 arcsec, respectively, yielding a level of contamination of about 10% due to our conservative pairing. We now proceed to further constrain their membership based on other colour-magnitude diagrams.

4.4 Red-optical Z-band photometry

We investigated the position of the YJ candidates in the $(Z - J, Z)$ diagram to further assess their membership (left-hand side panel in Fig. 3). We found 153 sources (out of 157) with *Z*-band photometry

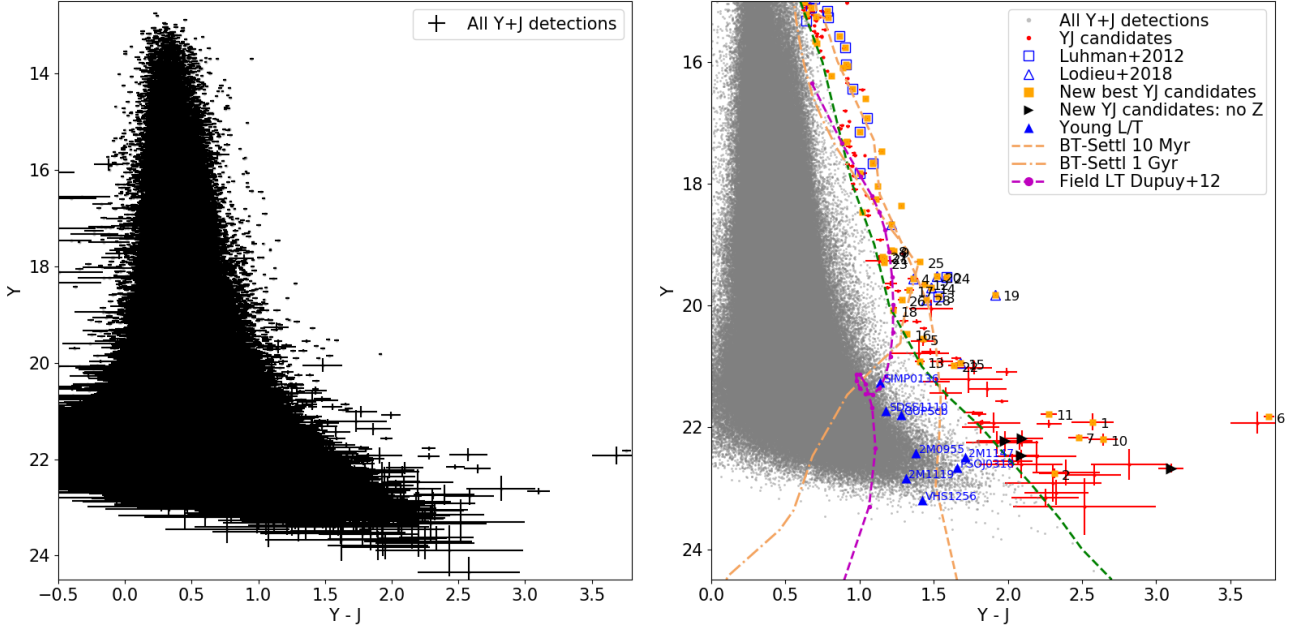


Figure 2. *Left:* $(Y - J, Y)$ colour-magnitude diagram for all Y, J sources in the two VISTA surveys with their error bars. *Right:* Same as left but with the addition of known USco members (blue open symbols) from [Luhman & Mamajek \(2012\)](#) and [Lodieu et al. \(2018a\)](#). The thick green line depicts our YJ photometric selection criterion. Red symbols highlight the new YJ candidates after applying our photometric selection (Section 4.3), whereas the orange symbols and black triangles show our best candidates that deserve spectroscopic follow-up. Their ID numbers from the first column of the tables in Appendix A are also indicated. The orange dashed lines represent the BT-Settl models for ages of 10 Myr dashed and 1 Gyr (dot-dashed). The purple line depicts the sequence of field L and T dwarfs from [Dupuy & Liu \(2012\)](#). Filled blue triangles and squares show known L and T dwarf members of young moving groups and the Pleiades, respectively.

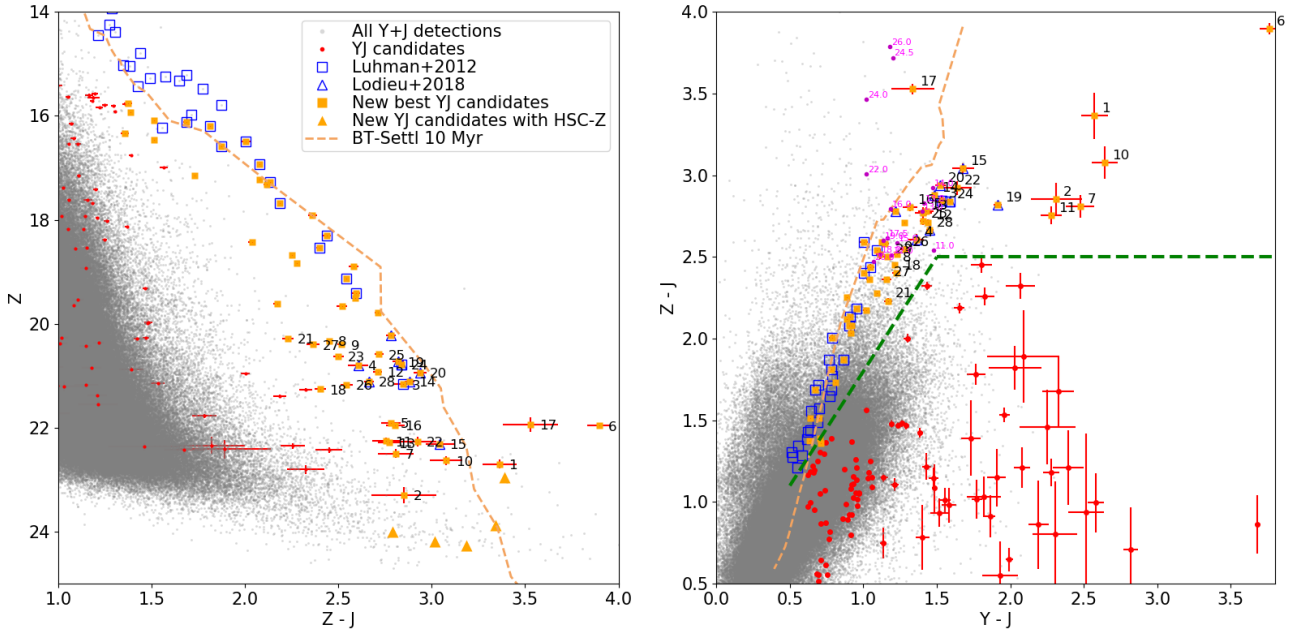


Figure 3. *Left:* $(Z - J, Z)$ colour-magnitude diagram for YJ candidates with Z -band detections (grey dots). Blue open squares and triangles are known USco members from [Luhman & Mamajek \(2012\)](#) and [Lodieu et al. \(2018a\)](#). The dashed brown line depicts the 10 Myr-old isochrone from [Baraffe et al. \(2015\)](#). Red dots highlight USco member candidates after applying the selection in the $(Y - J, Y)$ diagram. Orange and black symbols highlight our best L/T transition candidates for future spectroscopic follow-up. *Right:* $(Y - J, Z - J)$ colour-colour diagram with the same legend of symbols.)

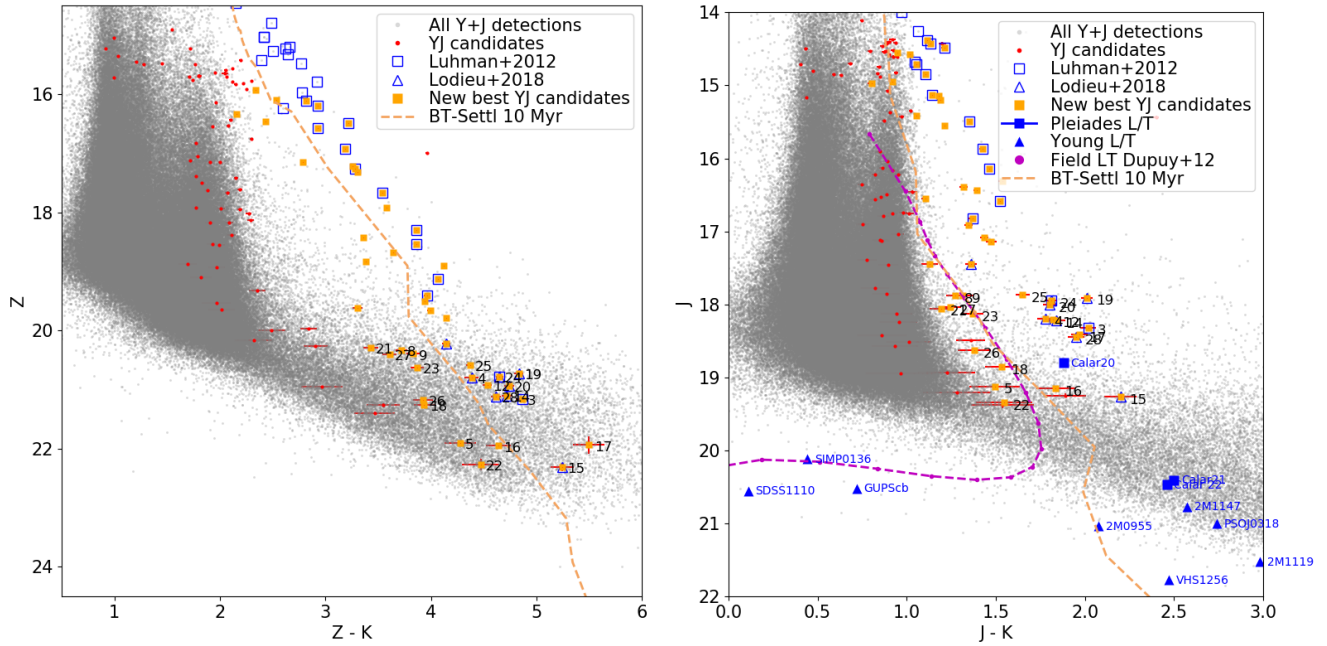


Figure 4. $(Z - K, Z)$ and $(J - K, J)$ colour-magnitude diagrams for YJ candidates with Z -band photometry and K -band counterparts from the UKIDSS GCS DR10. Red squares and blue triangles are known USco members from [Luhman & Mamajek \(2012\)](#) and [Lodieu et al. \(2018a\)](#). Orange symbols and black triangles highlight our final candidates after applying filtering in the YJ , ZJ , and ZK colours. The purple line with dots represents the sequence of field M, L, and T dwarfs ([Dupuy & Liu 2012](#)). The filled blue triangles show three L7–L8 members of TWA ([Gagné et al. 2017a](#)) and SIMP J013656.5+093347 a member of the 200 Myr-old Carina-Near moving group ([Gagné et al. 2017b](#)). The filled blue squares mark the position of the Pleiades member candidates Calar 20, 21, and 22 ([Zapatero Osorio et al. 2014c](#)).

from the first epoch of our original VISTA ZYJ survey, the remaining four are Z dropouts.

Fig. 3 depicts the $(Z - J, Z)$ diagram with the same symbols as the $(Y - J, Y)$ diagram. We observe that the sequence of members is well defined and becomes redder down to $Z \sim 20$ mag, as confirmed by the compilation of members of [Luhman & Mamajek \(2012\)](#) and highlighted in our previous studies (e.g. [Lodieu et al. 2006, 2007a; Lodieu 2013](#)). Beyond, the sequence seems to flatten with a relatively constant $Z - J$ colour and an increased dispersion that might be due to a combination of physical spread and large error bars at those faint magnitudes or intrinsic physical properties of such objects (dust, cloud decks).

We show the $(Y - J, Z - J)$ colour-colour diagram in the right panel of Fig. 3. Based on known members, we can see the USco sequence. We designed two straight lines to discard photometric non-members based on these two colours (green dashed lines in the right panel of Fig. 3): the first one goes from $(Y - J, Z - J) = (0.5, 1.1)$ to $(1.5, 2.5)$ mag while the second one excludes all sources with $Z - J$ colours bluer than 2.5 mag. The former is driven by the position of bright USco members from [Luhman & Mamajek \(2012\)](#) while the limit on the $Z - J$ colour corresponds to the reddest field M dwarfs in the solar neighbourhood ([Schmidt et al. 2010](#)). These selection criteria led to 57 bona-fide members highlighted with orange squares in all figures in this manuscript (Table A1).

In [Lodieu et al. \(2018a\)](#) we presented follow-up optical imaging in the Sloan i filter on the OSIRIS instrument (Optical System for Imaging and low Resolution Integrated Spectroscopy; [Cepa et al. 2000](#)) installed on the Gran Telescopio de Canarias (GTC) in La Palma (Canary Islands). The observations were taken as part of programme GTC4-14A during the month of August 2014 over several days under variable conditions resulting in inhomogeneous depths (Fig. 1). We

refer the reader to that paper for the logs of the observations and the description of the data reduction and analysis. We found 10 YJ candidates covered by the GTC observations, nine previously published in [Lodieu et al. \(2018b\)](#) and one new. This yet-unpublished SDSS i photometry of VISTA J16125313–2146274 further confirms this source as a member with a $i - J$ colour of 2.36 ± 0.02 mag (SDSS $i = 17.337 \pm 0.003$ mag; $J = 14.977 \pm 0.020$ mag), in agreement with the expected sequence of USco members.

Among the four ($157 - 153 = 4$) Z dropouts listed in Table A3 in Appendix A, none have additional photometric information from large-scale surveys such as UKIDSS GCS DR9, AllWISE or PanStarrs. We have checked the images of these databases and confirm that those positions are void of sources down to their detection limits. None of these four candidates appear in the unWISE catalogue of [Schlafly et al. \(2019\)](#). Their Y and J magnitudes range from 22.18–22.67 mag and 19.57–20.37 mag, respectively. Except for the source covered by the Subaru survey, we cannot further constrain the membership of these sources so they remain possible candidates. Nonetheless, we have checked the deep Y images as well the first VISTA Z, J epoch and can say the following about each object:

- 16:09:13.79 –23:35:46.9 ($J = 20.25$) lies in the halo of a bright star and might not be a real detection. We cast doubt on the membership of this source to USco.
- 16:04:46.7 –22:52:41.4 ($J = 20.37$) looks double in the J images while the Y image shows a single source. The object remains undetected in Z and in the UKIDSS images.
- 16:06:26.99 –22:50:00.6 ($J = 20.09$) lies in the halo of a bright star but the detections in Y and J are clear. The object is undetected in Z and in the images of the UKIDSS GCS. This object remains as a good candidate.
- 16:14:41.41 –22:16:29.8 ($J = 19.57$) looks double in the J im-

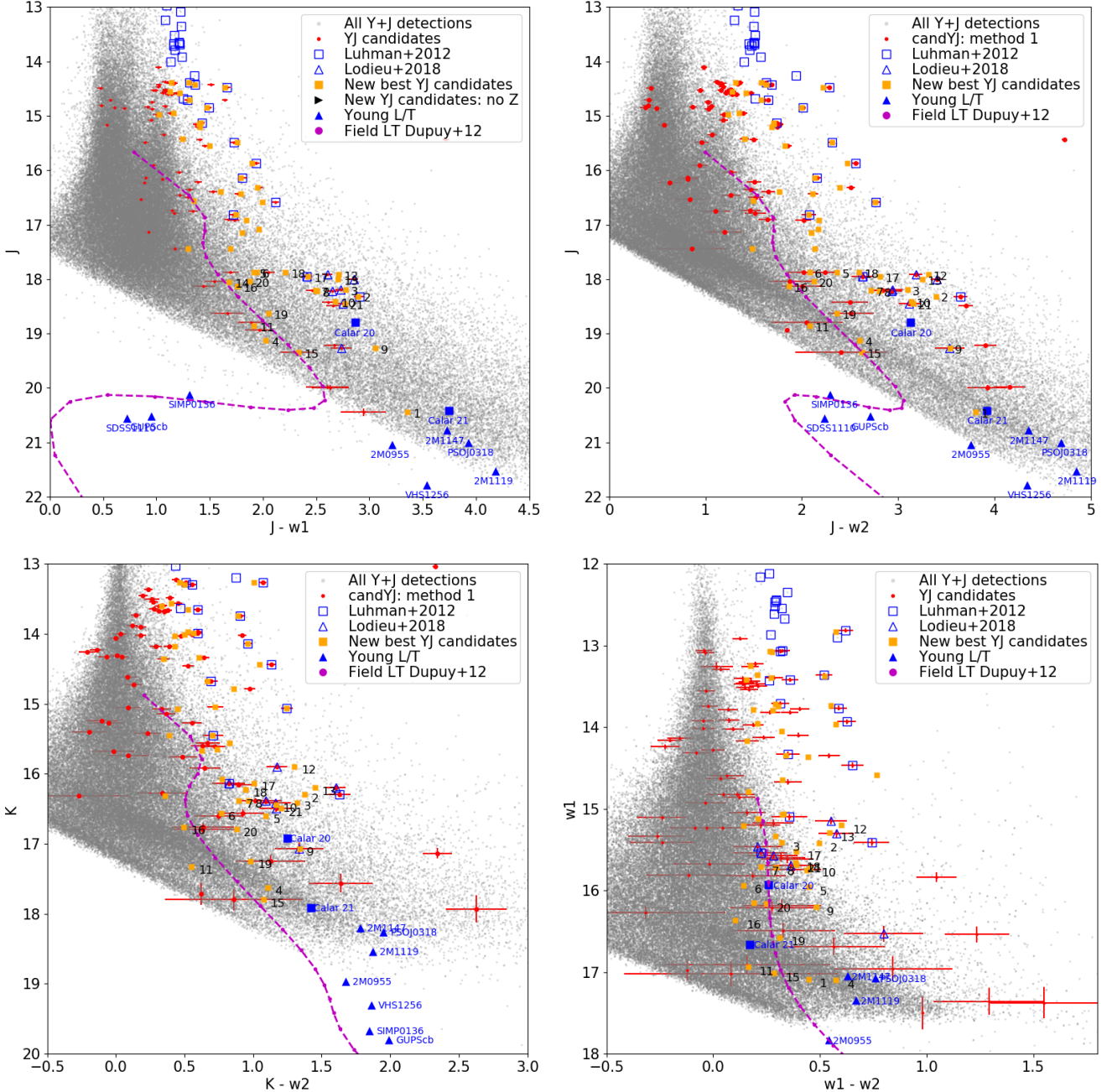


Figure 5. Colour-magnitude diagrams displaying all YJ candidates with Z -band photometry and UKIDSS GCS DR10 and AllWISE/unWISE counterparts. Red squares and blue triangles are known USco members from [Luhman & Mamajek \(2012\)](#) and [Lodieu et al. \(2018a\)](#). Orange symbols highlight our final candidates after applying filtering in the YJ , ZJ , and ZK colours. Orange symbols and black triangles highlight our best candidates with unWISE photometry. The purple line with dots represents the sequence of field M, L, and T dwarfs ([Dupuy & Liu 2012](#)). The blue filled triangles show three L7–L8 members of TWA ([Gagné et al. 2017a](#)) and SIMP J013656.5+093347 a member of the 200 Myr-old Carina-Near moving group ([Gagné et al. 2017b](#)) while the blue filled squares mark the position of the Pleiades member candidates Calar 20, 21, and 22 ([Zapatero Osorio et al. 2014c](#)).

ages while the Y image shows a single source. This is a similar case as the candidate in the second bullet above (16:04:46.7–22:52:41.4). The object is undetected in the in UKIDSS GCS but is detected as a point source in the Subaru Z image with $Z = 22.959 \pm 0.025$ mag. Its position in the $(Y - J, Z - J)$ and $(Z - J, Z)$ diagrams adds credibility to its membership to the USco association.

Up to now, we have assumed that the USco sequence is clearly visible in the $(Y - J, Y)$ diagram and extend previous compilation

of astrometric and spectroscopic members. To take into account the blue $Y - J$ colours of field (Section 4.1) and young (Section 4.2) L/T transition brown dwarfs and the extra depth provided by the Subaru HSC survey, we also tried applying a very conservative photometric selection, keeping all sources satisfying $Y - J \geq 0.9$ mag and $Y \geq 19.5$ mag undetected in the first VISTA Z -band epoch. This selection returned 4248 sources, of which 899 have an entry in the HSC catalogue but only 404 have good quality photometry or are

unsaturated. Placing these sources in the $(Y - J, Z - J)$ diagram, we observed that five remain as potential candidates because of their positions in the diagrams involving ZYJ photometry (Table A2 in Appendix A). However, only two of these five (the two brightest in Z) appear as most likely members because they extend the current sequence of members in the $(Z - J, Z)$ and $(Y - J, Z - J)$ diagrams (Fig. 3). We emphasise that the HSC survey covers only 1.5 square degrees and that we recover only $\sim 20\%$ (899 out of 4248) of the sources without VISTA Z photometry. Hence, the number of potential L/T transition members in USco might be five times larger, fact that we should consider when discussing the luminosity function (Section 6.2).

4.5 Infrared photometry

The YJ candidates with Z -band photometry not rejected in the $(Y - J, Z - J)$ diagram, which turns out to be one of the best diagrams to discriminate members from contaminants, remain as potential members in diagrams involving near- and mid-infrared photometry from the UKIDSS GCS DR9, AllWISE, and unWISE catalogues, respectively (Fig. 4 and Fig. 5). However, we point out that eight sources with the following ID might be non members based on their positions in several of these diagrams with infrared photometry: #5, 8, 9, 18, 21, 22, 23, 26, and 27. However, we can not entirely discard them as potential members because L/T field transition dwarfs show a significant dispersion in the $Y - J$ and $Z - J$ colours that we observe in this part of the sequence (Fig. 4).

As mentioned in the previous Section 4.4, only one of the four YJ candidates without VISTA Z detections has additional photometry from our Subaru deep survey and remains as bona-fide candidate. The other three sources do not appear in the infrared CMDs (Fig. 4–5).

Finally, as mentioned earlier, the depth of the K and $w1, w2$ surveys are generally insufficient to detect counterparts to our faintest candidates, especially those with Z -band photometry from the deep HSC survey, and allow for a fair comparison with the locations of the young T-type brown dwarfs in colour-magnitude diagrams. Nonetheless, we find two of the 10 HSC Z detections (but VISTA Z dropouts) in AllWISE, adding credit to their membership because they follow the empirical USCo sequence (Fig. 5).

4.6 Proper motions

We calculated the proper motion in right ascension and declination of the YJ candidates comparing the positions between the J -band first epoch and the Y -band second epoch assuming a mean baseline of 4.15 years. We ignore the Z and Y first epochs because they are shallower and do not include a detection for all the YJ candidates. We calculated the mean dispersion of the full sample of several hundred thousands Y and J detections in both directions to estimate the error bars on the proper motions of the faintest candidates in our sample. We find median absolute deviation values below 10.2 and 9.5 mas/yr for sources brighter than $Y = 21$ mag in right ascension and declination, respectively. The deviations increase to values of about 15 mas/yr, 30 mas/yr, and 135 mas/yr in both directions in the $Y = 21$ –22, 22–23, 23–24 mag intervals, respectively, and represent upper limits. We note that the mean values of the proper motions are -1.90 and 0.33 mas/yr in right ascension and declination, respectively, hence very close to the expected nominal centre at $(0,0)$.

We cross-matched the list of 863 members from [Luhman & Mamajek \(2012\)](#) with the full VISTA catalogue to estimate the mean proper

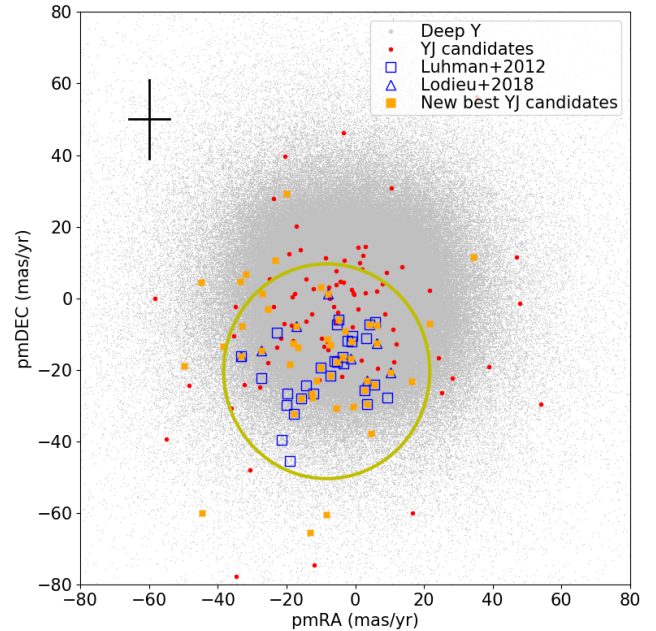


Figure 6. Vector point diagram with the proper motions in the right ascension and declination (in mas/yr) of the YJ candidates (red dots). Typical error bars are drawn in the top left corner. Blue squares and triangles are known USCo members from the compilation of [Luhman & Mamajek \(2012\)](#) and [Lodieu et al. \(2018a\)](#). Orange symbols highlight our final candidates after applying filtering in the YJ , ZJ , and ZK colours.

motion of USCo members from the 4.15 year baseline between the two VISTA epochs, yielding $(\mu_\alpha \cos \delta, \mu_\delta) = (-8.3, -20.4)$ mas/yr based on 29 sources in common to the area surveyed by our deep Y survey. These mean values agree well with the mean values of the Hipparcos ([de Bruijne et al. 1997](#); [de Zeeuw et al. 1999](#)) and *Gaia* ([Luhman & Esplin 2020a](#)) astrometric missions but with larger uncertainties as expected for ground-based proper motions.

We list the proper motions for our candidate members in the last two columns of Table A1 in Appendix A and show the vector point diagram zoomed on a central part in Fig. 6. The distribution of the best candidates, i.e. those remaining after applying filters based on $Z - J$ and $Z - K$ colours, appears to shift towards the expected mean cluster motion in the vector point diagram when compared with candidates from YJ colours alone. We observe that most of our photometric candidates lie within a 3σ circle centered on the mean proper motion of previous members (yellow circle in Fig. 6). Among the sources brighter than $Y = 19$ mag, we would reject 5 and 1 source(s) applying a 3σ and 5σ selection, respectively. The astrometric selection would thus suggest a level of contamination of approximately 3.4–17.2% among the 29 sources brighter than $Y = 19$ mag. Hence, we can clear discard VISTA J16105178–233327.4 but leave the other four sources as potential candidates. In the $Y = 19$ –20 mag range where the median absolute deviations in proper motions remain below 10 mas/yr, we would reject four sources outside 3σ , one of them being outside the 5σ limit, VISTA J16153235–2259510. At faint magnitudes, we find six objects with very large proper motions but we do not discard them as member candidates at this stage because they lie at the limit of our deep Y survey with magnitudes fainter than 21.7 mag. The median absolute deviations increase drastically beyond $Y = 22$ mag, as reported above.

5 SPECTROSCOPIC OBSERVATIONS

5.1 VLT/X-shooter near-infrared spectroscopy

5.1.1 Spectroscopic observations

We conducted spectroscopy of two candidates with the X-shooter (D’Odorico et al. 2006; Vernet et al. 2011) instrument on the ESO Very Large Telescope (VLT) Unit 2 in visitor mode on the night of 7 May 2018 (programme 0101.C-0565; PI Lodieu). The combination of the faintest of the targets, time allocation, and weather conditions allowed us to collect spectra for only two of our photometric candidates with sufficient signal-to-noise for spectral classification (Table 2). X-shooter is a multi-wavelength cross-dispersed echelle spectrograph equipped with three independent arms observing simultaneously in the ultraviolet (UVB; 0.3–0.56 μm), visible (VIS; 0.56–1.02 μm), and near-infrared (NIR; 1.02–2.48 μm) whose light is split by two dichroics. The UVB, VIS, and NIR arms are equipped with a 4096×2048 E2V CCD44-82, a 4096×2048 MIT/LL CCID 20 detectors, and a 2096×2096 Hawaii 2RG array, respectively.

We set the instrument configuration to a read-out mode of 400k with low gain and no binning. We employed the 1.3 arcsec slit in the UVB and 1.2 arcsec slits in the VIS and NIR, resulting in nominal resolving powers of 4000 (8.1 pixels per FWHM), 6700 (7.9 pixels per FWHM), and 3900 (5.8 pixels per FWHM) in the UVB, VIS, and NIR arms, respectively. We set the individual integration times to 300 sec in the NIR arm and repeated the AB patterns multiple times to optimize the sky subtraction in the infrared. We carried out all observations with the slit aligned with the parallactic angle. We acquired both targets by pointing to a bright star located at less than 30 arcsec and applied an offset in both right ascension and declination calculated from the coordinates measured on the VISTA images. We give the logs of spectroscopic observations in Table 2, where we list coordinates, the new Y magnitudes, date of the observations, number of exposures, and exposure times set in the NIR arm for both targets.

5.1.2 Spectroscopic data reduction

We downloaded the reduced 2D spectra of the two targets from the ESO science archive (Table 2). The data reduction is made automatically with the `esoreflex` pipeline and includes 2D and 1D spectra extracted optimally without telluric correction. We did not detect any signal in the UVB arm and no obvious emission line like $H\alpha$ in the VIS spectra of both targets, except for extremely weak signals beyond 900 nm, hence, we concentrate our analysis on the NIR arm. We removed tellurics from the NIR spectra of both targets with the `molecfit` package distributed by ESO (Kausch et al. 2015; Smette et al. 2015)¹. The final spectra are shown in Fig. 7 with the smoothed spectra by a factor of 21 pixels (black) on top of the unsmoothed spectra displayed in grey.

5.2 Near-infrared spectral classification

We inspected the X-shooter infrared spectra displayed in Fig. 7, which reveal the presence of spectral features typical of young (i.e. low gravity) L dwarfs: a strong VO band at 1.06 micron, the triangular shape in the H -band, weak alkali lines like the KI potassium doublets at 1.169/1.177 and 1.243/1.252 microns, and strong water bands (Martín et al. 1996; Luhman et al. 1998; Zapatero Osorio

Table 2. Logs of the VLT X-shooter spectroscopic observations. We provide the identified number (Table A1), coordinates (J2000) of the targets, their Y -band magnitudes, the date of observations, and the number and length of the on-source integrations employed for the NIR arm.

ID	RA (J2000)	dec (J2000)	Y	Date	ExpT
	hh:mm:ss.ss	dd:’:”	mag	yyyy-mm-dd	sec
15	16:06:09.23	−23:38:11.4	18.034±0.005	2018-05-07	6×300
36	16:11:10.31	−21:45:16.5	19.745±0.015	2018-05-07	12×300

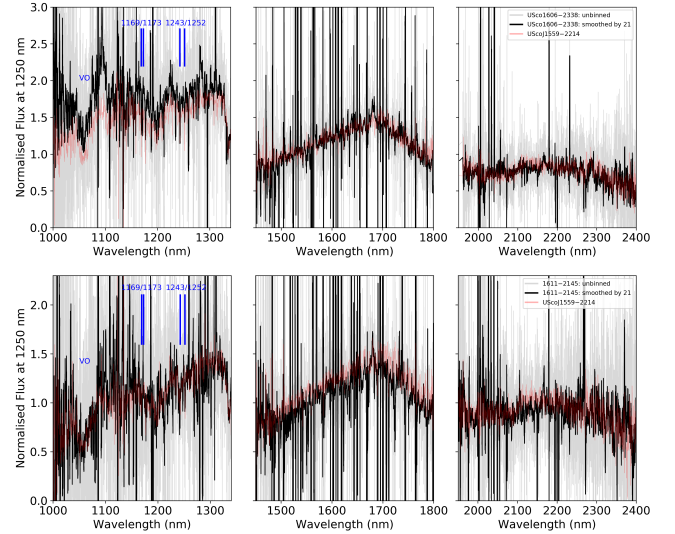


Figure 7. VLT X-shooter spectra of two of our best photometric candidates. Top figure: we plot USco 16060923–2338114 (ID15) compared to the known L1 dwarf USco J155936–221415. Bottom figure: we overplot the known L6 dwarf USco 160413–224103 on top of USco 16111031–2145165 (ID36). We highlight the positions of the VO band at 1.06 microns and the two potassium doublets in the J -band panel, both sensitive to gravity.

et al. 2000; Lucas & Roche 2000; Gorlova et al. 2003; McGovern et al. 2004; Kirkpatrick 2005; Cruz et al. 2009; Allers & Liu 2013; Alves de Oliveira et al. 2013; Bonnefoy et al. 2014; Manjavacas et al. 2014; Mužić et al. 2014; Lodieu et al. 2018a; Chinchilla et al. 2020). We performed the spectral classification of the two sources by direct comparison with known L0–L7 dwarf members of the USco association collected with the same VLT/X-shooter set-up (Lodieu et al. 2018a) and Gemini Near-Infrared Spectrograph GNIRS (Elias et al. 2006; Lodieu et al. 2008). We infer infrared spectral types of $L1.0\pm 0.5$ and $L6\pm 1.0$ for USco J16060923–2338114 and USco J16111031–2145165, respectively.

We investigated the strengths of the KI potassium doublets present in the J -band region of the spectra for both objects (left panels in Fig. 7). We set upper limits of 0.01 nm on the doublet at (1169.0, 1173.3) nm. We derived pseudo-equivalent widths of $(0.031\pm 0.005, 0.019\pm 0.04)$ and $(0.014\pm 0.001, 0.024\pm 0.03)$ nm and for the potassium doublet further to the red with central wavelengths of (1242.99, 1252.31) and (1243.14, 1252.15) nm, for ID98600 and ID341056, respectively. These values are in agreement with weak potassium features seen in USco L0–L7 dwarfs (Peña Ramírez et al. 2016; Lodieu et al. 2018a).

¹ <http://www.eso.org/sci/software/pipelines/skytools/molecfit>

6 DISCUSSION AND IMPLICATIONS

6.1 Did we really find T-Type members?

Old field T dwarfs are brown dwarfs whose infrared spectra are shaped by strong methane and water bands as well as H₂ collision-induced absorption (Leggett et al. 2000; Burgasser et al. 2002; Geballe et al. 2002; Burgasser et al. 2006). Their optical spectra are dominated by pressure-broadened alkali lines (Burgasser et al. 2003). The dust present in L dwarfs has settled at the bottom of their atmospheres, resulting in red optical and optical-to-infrared colours but blue near-infrared colours. Their effective temperatures are typically below 1300 K.

In view of the numbers of possible candidate members left after applying the difference colours cuts, we discuss the chances that these might be T-type dwarfs belonging to USco. Based on photometry and colours, field L and T dwarfs display constant $Y - J$ colours with some significant scatter (Hewett et al. 2006; Lodieu et al. 2007b; Pinfield et al. 2008; Burningham et al. 2010, 2013), opposite to the sequence of USco member candidates identified in the $(Y - J, Y)$ colour-magnitude diagram (Fig. 2). We observe that the $Y - J$ colours of potential late-L/early-T member candidates is not constant but rather becoming redder with fainter magnitudes. This is expected for members of a cluster or association that follow a sequence, with the coolest members exhibiting the latest spectral types.

The $Z - J$ colours of field L/T dwarfs remain relatively constant, consistent with most of our USco candidates. Nonetheless, we identified a few sources with distinct $Z - J$ colours compared to other USco candidates (Fig. 3). On the one hand, USco J1611015–21451693 (#17) is very red in $Z - J$ but rather blue in $Y - J$. On the other hand, USco J16051784–23355193 (#6) shows red colours on both axes and seems to extend a sequence marked by a small group of sources (#1, 2, 7, 10, 11). Based on their magnitudes, #17 is as bright as the mid-L dwarfs confirmed spectroscopically while #6 is among the faintest of our candidates and lies at the bottom of the sequence. Consequently, we suggest that one of these two new candidates might be a true T-type member in USco. However we have neither additional photometry nor spectroscopy for it so we cannot yet make a strong case.

Furthermore, the sequence of old L and T dwarfs turns to the blue across the L/T transition in the $J - K$ colour (purple dashed line in Fig. 4) based on the absolute magnitude vs spectral type relations of Dupuy & Liu (2012) in the Mauna Kea Observatory system as well as the $J - w1$ and $J - w2$ colours whereas it keeps redder in the $K - w2$ and $w1 - w2$ colours (purple line in Fig. 5). Unfortunately we do not observe a kink in the USco sequence in those diagrams, most likely due to the limited depth of the UKIDSS Galactic Clusters Survey in the K -band (100% completeness of about 18.2 mag) and the AllWISE/unWISE catalogues that do not provide any detection for our faintest candidates. This suggests that our survey has not yet uncovered T-type planetary-mass objects in USco.

Moreover, we note that the J -band magnitudes of the faintest candidates are similar because the Y magnitudes become fainter and the $Y - J$ redder at the same time. Consequently, their absolute magnitudes should be comparable, which we would expect if the trend is consistent with field L6–T4 dwarfs having J -band absolute magnitudes that differ by less than a few tens of magnitudes (Dupuy & Liu 2012). Hence, the new candidates might well be late-L dwarfs but could also have later spectral types (e.g. cases of #6 and #17).

Did we really find young T-type planetary-mass members in USco? The answer is undecided (i.e. *maybe*) because we lack unambiguous evidence in spite of being two magnitudes fainter in Y and having identified candidates one magnitude fainter in J than late-

L dwarfs confirmed spectroscopically. Nonetheless, we highlight USco J16051784–23355193 (#6) as a potential USco T-type member due to its extreme $Y - J$ and $Z - J$ colours that differ from other candidates and that an increase in redness. Moreover, we cannot discard USco J1611015–21451693 (#17) as a T-type member because it shows red $Z - J$ colours consistent with the synthetic colours of old field T dwarfs (Hewett et al. 2006). However, further photometry and spectroscopy are needed to confirm both as young T dwarfs.

6.2 The USco IMF in the planetary-mass regime

The aim of this subsection is to discuss the shape and form of the USco luminosity and mass functions into the planetary-mass regime. In Table 3, we give the final numbers of YJ candidates before and after rejection of potential photometric non members, equivalent to the luminosity function (Fig. 8). We transform the luminosity function into a mass spectrum, assuming an age of 10 Myr (Pecaut et al. 2012) and the magnitude-mass relation from the BT-Settl model (Baraffe et al. 2015). We also specify the mass range according to the BT-Settl 10 Myr-old isochrone in Table 3. We assumed an age of 10 Myr for USco based on the comparison of these models with the masses derived from eclipsing binaries identified in the association thanks to the Kepler K2 mission (Borucki et al. 2010; Lissauer et al. 2014; Batalha 2014) over the past years (Alonso et al. 2015; Kraus et al. 2015; Lodieu et al. 2015; David et al. 2016b, 2019). The BT-Settl models at 10 Myr reproduce relatively well the sequence of USco eclipsing binaries in the mass-radius diagram (Lodieu et al. 2020). The age of USco might well be as young as 5 Myr from isochrone fitting of the lowest mass stars (Preibisch & Zinnecker 1999; Preibisch et al. 2001; Song et al. 2012; David et al. 2019) with an upper limit of about 10 Myr (Pecaut et al. 2012).

In Table 3 we observe that the number of objects per bin of magnitudes in the six square degrees is relatively constant over the $J = 14$ – 20 mag range. We considered Poissonian errors on the luminosity function taking the square root of the number of objects in each column that we need to sum up to obtain the total number of candidates per magnitude bin. This is as a very approximate but recommended practice to estimate the error bars in histograms². The last two bins are incomplete because our J -band survey is 100% complete down to $J = 20.5$ mag. Typically we find 1.0–1.5 planetary-mass member per square degree in this area of USco, up to two maximum. We observe an increase in the planetary-mass regime if all photometric YJ candidates are bona-fide members. If only the smallest numbers of candidates is confirmed with further follow-ups, the shape of the mass spectrum would rather be flat in the 20–7 M_{Jup} range. We can discard a significant decrease in the numbers of members down to 5 M_{Jup} , assuming an age of 10 Myr, unless all photometric candidates are rejected in the future. If the age of USco is 5 Myr, the lower mass limit of our survey would be just below 4 M_{Jup} . In spite of all uncertainties associated to models at these low masses and young ages as well as the lack of spectroscopic confirmation, star formation processes can form isolated planetary-mass objects down to 5 M_{Jup} , consistent with the findings in the solar neighbourhood (Kirkpatrick et al. 2019).

² https://docs.astropy.org/en/stable/api/astropy.stats.poisson_conf_interval.html

Table 3. Numbers of new YJ candidates per bin of J magnitudes. We list the total number of objects (= luminosity function) in the area of six square degrees covered by our deep Y survey. We give the numbers of YJ candidates before (YJ) and after rejection (Rej) based on their position in diagrams involving additional passbands. We also list the four candidates undetected in the VISTA Z survey (noZ) and those remaining as potential candidates from the deep HSC survey (HSCZ). We take into account that the Subaru survey covers only 20% of the VISTA survey, resulting in a factor of five to consider when counting the number of potential candidates after applying the selection in the z -band. The final number (or range) of objects (dN) is the sum of columns 2, 4, and 5 minus the number of rejected candidates in column 3. We give in parenthesis the range of values considering the Poissonian statistics rounded to the nearest decimal. The mass range is computed using the BT-Settl 10 Myr-old isochrones. The last column gives the number of objects per mass bin rounded to the nearest integer, dividing dN by the difference of the mass range with its associated Poissonian interval in parenthesis. We warn that the first and last two bins are incomplete due to saturation at bright magnitude and the 100% completeness at $J = 20.5$ mag, respectively.

J	YJ	Rej	noZ	HSCZ	dN	Mass range	dN/dM
mag	M_{\odot}						
14–15	10	0	0	0	10 (6.8–13.1)	0.0600–0.0220	263 (247–279)
15–16	7	1	0	0	6 (3.5–8.5)	0.0220–0.0160	1000 (968–1032)
16–17	8	3	0	0	5 (2.7–7.2)	0.0160–0.0120	1250 (1214–1285)
17–18	9	3	0	0	6 (3.5–8.5)	0.0120–0.0095	2400 (2351–2449)
18–19	13	5–8	0	0	5–8 (2.7–10.3)	0.0095–0.0073	2242–3587 (2194–3647)
19–20	9	0	0–1	1×5	14–15 (8.1–20.9)	0.0073–0.0059	10000–10714 (5786–14929)
20–21	1	0	1–2	1×5	7–8 (1.5–13.5)	0.0059–0.0045	5000–5714 (1071–9643)
21–22	0	0	0	(2±1)×5	≥(5–15) ≥(2.9–17.1)	0.0045–0.0037	≥6250–18750 (3625–21375)

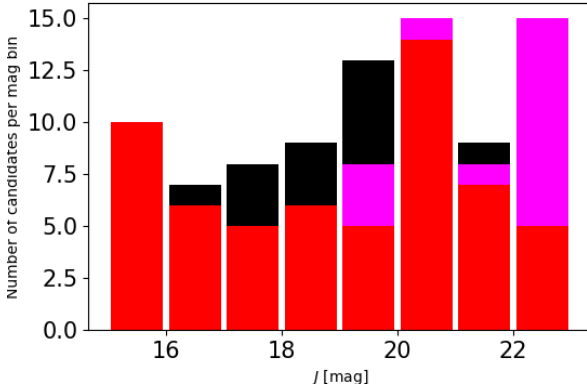


Figure 8. Luminosity function: numbers of new YJ candidates in the $J = 14$ – 21 mag interval before rejection of potential photometric non members (black). The red and magenta histograms indicate the minimum and maximum numbers of YJ candidates after rejection of potential photometric non members (Table 3). The first and last two bins are incomplete due to saturation at bright magnitude and the 100% completeness at $J = 20.5$ mag, respectively.

7 CONCLUSIONS AND FUTURE WORK

We presented a dedicated photometric search in $\sim 6 \text{ deg}^2$ in the central region of the USco association to look for the coolest members with a special focus on late-L and T-type candidates. Our survey is the deepest in the association over such large area, between 2 and 1 magnitude deeper in Y and J than any previous study and we are now closer to reach the regime of T dwarfs in USco. The main results of our study are:

- We identified 10 new candidates fainter than the previously known L7 members confirmed spectroscopically. Their magnitudes are fainter than $Y = 21.7$ mag ($J > 19.5$ mag), equivalent to masses below $5 M_{\text{Jup}}$ according to evolutionary models at an age of 10 Myr.

- We highlight two potential T-type member candidates among the 10 faintest sources identified in our deep survey.
- We derived proper motion confirmation of the brightest member candidates while the accuracy of the astrometry is limited for the newest and faintest candidates.
- We presented near-infrared spectroscopy of two photometric candidates confirmed them as young L dwarfs, adding credence to their membership. The remaining candidates require optical and/or infrared spectroscopic follow-up.
- We derive photometric estimates of the luminosity function and mass spectrum in the planetary-mass domain showing no obvious sign of dearth of members down to masses of $5 M_{\text{Jup}}$. Although this analysis is preliminary and requires photometric and spectroscopic follow-ups, there is now growing observational evidence that the star formation processes can form isolated objects with masses below $5 M_{\text{Jup}}$ in the field and in young regions.

ACKNOWLEDGMENTS

NL was partly funded by the programme AYA2015-69350-C3-2-P from Spanish Ministry of Economy and Competitiveness (MINECO) and acknowledges support from the Agencia Estatal de Investigación del Ministerio de Ciencia e Innovación (AEI-MCINN) under grant PID2019-109522GB-C53. NL has benefited from internal funding from an IAC Severo Ochoa outgoing fellowship for a stay at the Royal Observatory in Edinburgh. We warmly thank the staff at the Royal Observatory Edinburgh and Cambridge Astronomy Survey Unit for their valuable help and support with the data reduction, in particular Mike Read, Rob Blake, Eckhard Sutorius, Mike Irwin, Aybuke Kupcu Yoldas, and Carlos González-Fernández.

This research has made use of the Simbad and VizieR (Ochsenbein et al. 2000) databases, operated at the Centre de Données Astronomiques de Strasbourg (CDS), and of NASA’s Astrophysics Data System Bibliographic Services (ADS).

Based on observations collected at the European Organisation for Astronomical Research in the Southern Hemisphere under ESO programme(s) 095.C-0781(A), 089-C.0102(ABC), and 0101.C-0565.

This work is based on programmes GTC4-14A (PI Lodieu) made

with the Gran Telescopio Canarias (GTC), operated on the island of La Palma in the Spanish Observatorio del Roque de los Muchachos of the Instituto de Astrofísica de Canarias.

This work is partly based on data collected at Subaru Telescope, which is operated by the National Astronomical Observatory of Japan.

Based on data from the UKIRT Infrared Deep Sky Survey (UKIDSS). The UKIDSS project is defined in [Lawrence et al. \(2007\)](#) and uses the UKIRT Wide Field Camera (WFCAM; [Casali et al. 2007](#)). The photometric system is described in [Hewett et al. \(2006\)](#) and the calibration is described [Hodgkin et al. \(2009\)](#). The pipeline processing and science archive are described in [Irwin et al. \(2009, in prep\)](#) and [Hambly et al. \(2008\)](#).

The Pan-STARRS1 Surveys (PS1) have been made possible through contributions of the Institute for Astronomy, the University of Hawaii, the Pan-STARRS Project Office, the Max-Planck Society and its participating institutes, the Max Planck Institute for Astronomy, Heidelberg and the Max Planck Institute for Extraterrestrial Physics, Garching, The Johns Hopkins University, Durham University, the University of Edinburgh, Queen's University Belfast, the Harvard-Smithsonian Center for Astrophysics, the Las Cumbres Observatory Global Telescope Network Incorporated, the National Central University of Taiwan, the Space Telescope Science Institute, the National Aeronautics and Space Administration under Grant No. NNX08AR22G issued through the Planetary Science Division of the NASA Science Mission Directorate, the National Science Foundation under Grant No. AST-1238877, the University of Maryland, and Eotvos Lorand University (ELTE).

This publication makes use of data products from the Wide-field Infrared Survey Explorer, which is a joint project of the University of California, Los Angeles, and the Jet Propulsion Laboratory/California Institute of Technology, and NEOWISE, which is a project of the Jet Propulsion Laboratory/California Institute of Technology. WISE and NEOWISE are funded by the National Aeronautics and Space Administration.

John D. Hunter. Matplotlib: A 2D Graphics Environment, *Computing in Science & Engineering*, 9, 90-95 (2007), DOI:10.1109/MCSE.2007.55 (publisher link) Stefan van der Walt, S. Chris Colbert and Gaël Varoquaux. The NumPy Array: A Structure for Efficient Numerical Computation, *Computing in Science & Engineering*, 13, 22-30 (2011), DOI:10.1109/MCSE.2011.37 (publisher link) Jones E, Oliphant E, Peterson P, et al. SciPy: Open Source Scientific Tools for Python, 2001-, <http://www.scipy.org/> [Online; accessed 2017-10-03].

TOPCAT was initially (2003-2005) developed under the UK Starlink project (1980-2005, R.I.P.). Since then it has been supported by grant PP/D002486/1 from the UK's Particle Physics and Astronomy Research Council, the VOTech project (from EU FP6), the AstroGrid project (from PPARC/STFC), the AIDA project (from EU FP7), grants ST/H008470/1, ST/I00176X/1, ST/J001414/1 and ST/L002388/1 from the UK's Science and Technology Facilities Council (STFC), the GAVO project (BMBF Bewilligungsnummer 05A08VHA), the European Space Agency, and the FP7 project GEINIUS.

DATA AVAILABILITY

The data underlying this article will be made public to the community through Vizier at the Centre de Données de Strasbourg at <http://cdsweb.u-strasbg.fr>, and can be accessed with the bibcode or last name of the first author of the paper.

REFERENCES

- Allers K. N., Liu M. C., 2013, *ApJ*, **772**, 79
- Alonso R., Deeg H. J., Hoyer S., Lodieu N., Palle E., Sanchis-Ojeda R., 2015, *A&A*, **584**, L8
- Alves de Oliveira C., Moraux E., Bouvier J., Duchêne G., Bouy H., Maschberger T., Hudelot P., 2013, *A&A*, **549**, A123
- Ardila D., Martín E., Basri G., 2000, *AJ*, **120**, 479
- Baraffe I., Homeier D., Allard F., Chabrier G., 2015, *A&A*, **577**, A42
- Barsony M., Haisch K. E., Marsh K. A., McCarthy C., 2012, *ApJ*, **751**, 22
- Bastian N., Covey K. R., Meyer M. R., 2010, *ARA&A*, **48**, 339
- Batalha N. M., 2014, *Proceedings of the National Academy of Science*, **111**, 12647
- Béjar V. J. S., Zapatero Osorio M. R., Pérez-Garrido A., Álvarez C., Martín E. L., Rebolo R., Villó-Pérez I., Díaz-Sánchez A., 2008, *ApJL*, **673**, L185
- Best W. M. J., et al., 2017, *ApJ*, **837**, 95
- Boley A. C., Durisen R. H., 2010, *ApJ*, **724**, 618
- Bonnefoy M., Chauvin G., Lagrange A.-M., Rojo P., Allard F., Pinte C., Dumas C., Homeier D., 2014, *A&A*, **562**, A127
- Borucki W. J., et al., 2010, *Science*, **327**, 977
- Bosch J., et al., 2018, *PASJ*, **70**, S5
- Boss A. P., 1988, *ApJ*, **331**, 370
- Boyd D. F. A., Whitworth A. P., 2005, *A&A*, **430**, 1059
- Burgasser A. J., et al., 2002, *ApJ*, **564**, 421
- Burgasser A. J., Kirkpatrick J. D., Liebert J., Burrows A., 2003, *ApJ*, **594**, 510
- Burgasser A. J., Geballe T. R., Leggett S. K., Kirkpatrick J. D., Golimowski D. A., 2006, *ApJ*, **637**, 1067
- Burgess A. S. M., Moraux E., Bouvier J., Marmo C., Albert L., Bouy H., 2009, *A&A*, **508**, 823
- Burningham B., et al., 2010, *MNRAS*, **406**, 1885
- Burningham B., et al., 2013, *MNRAS*, **433**, 457
- Casali M., Adamson A., Alves de Oliveira C., Almaini O., Burch K., Chuter T., Elliot J., 23 co-authors 2007, *A&A*, **467**, 777
- Cepa J., et al., 2000, in M. Iye & A. F. Moorwood ed., Society of Photo-Optical Instrumentation Engineers (SPIE) Conference Series Vol. 4008, Society of Photo-Optical Instrumentation Engineers (SPIE) Conference Series. pp 623-631
- Chambers K. C., Magnier E. A., Metcalfe N., 103 co-authors 2016, *ApJ*,
- Chiang P., Chen W. P., 2015, *ApJL*, **811**, L16
- Chinchilla P., et al., 2020, *A&A*, **633**, A152
- Cook N. J., Scholz A., Jayawardhana R., 2017, *AJ*, **154**, 256
- Cross N. J. G., et al., 2012, *A&A*, **548**, A119
- Cruz K. L., Kirkpatrick J. D., Burgasser A. J., 2009, *AJ*, **137**, 3345
- Cutri R. M., et al. 2014, VizieR Online Data Catalog, **2328**, 0
- Cutri R. M., et al., 2013, Explanatory Supplement to the AllWISE Data Release Products, Explanatory Supplement to the AllWISE Data Release Products
- D'Odorico S., et al., 2006, in Society of Photo-Optical Instrumentation Engineers (SPIE) Conference Series. , doi:10.1117/12.672969
- Dalton G. B., et al., 2006, in Society of Photo-Optical Instrumentation Engineers (SPIE) Conference Series. , doi:10.1117/12.670018
- David T. J., et al., 2016a, *Nat*, **534**, 658
- David T. J., Hillenbrand L. A., Cody A. M., Carpenter J. M., Howard A. W., 2016b, *ApJ*, **816**, 21
- David T. J., Hillenbrand L. A., Gillen E., Cody A. M., Howell S. B., Isaacson H. T., Livingston J. H., 2019, *ApJ*, **872**, 161
- Davis L. E., 1999, in Craine E. R., Crawford D. L., Tucker R. A., eds, *Astronomical Society of the Pacific Conference Series Vol. 189, Precision CCD Photometry*, p. 35
- Dawson P., Scholz A., Ray T. P., 2011, *MNRAS*, **418**, 1231
- Dawson P., Scholz A., Ray T. P., Marsh K. A., Wood K., Natta A., Padgett D., Ressler M. E., 2013, *MNRAS*, **429**, 903
- Dawson P., Scholz A., Ray T. P., Peterson D. E., Rodgers-Lee D., Geers V., 2014, *MNRAS*, **442**, 1586
- Dupuy T. J., Liu M. C., 2012, *ApJS*, **201**, 19
- Elias J. H., Joyce R. R., Liang M., Muller G. P., Hileman E. A., George J. R., 2006, in *Ground-based and Airborne Instrumentation for Astronomy*.

- Edited by McLean, Ian S.; Iye, Masanori. Proceedings of the SPIE, Volume 6269, pp. (2006).. , doi:10.1117/12.671817
- Emerson J. P., 2001, in R. Clowes, A. Adamson, & G. Bromage ed., *Astronomical Society of the Pacific Conference Series* Vol. 232, *The New Era of Wide Field Astronomy*, p. 339
- Emerson J. P., Sutherland W. J., McPherson A. M., Craig S. C., Dalton G. B., Ward A. K., 2004, *The Messenger*, **117**, 27
- Faherty J. K., et al., 2016, *ApJS*, **225**, 10
- Filippazzo J. C., Rice E. L., Faherty J., Cruz K. L., Van Gordon M. M.,Looper D. L., 2015, *ApJ*, **810**, 158
- Forgan D., Rice K., 2011, *MNRAS*, **417**, 1928
- Furusawa H., et al., 2018, *PASJ*, **70**, S3
- Gagné J., et al., 2015a, *ApJS*, **219**, 33
- Gagné J., Lafrenière D., Doyon R., Malo L., Artigau É., 2015b, *ApJ*, **798**, 73
- Gagné J., et al., 2017a, *ApJS*, **206**, 18
- Gagné J., et al., 2017b, *ApJL*, **841**, L1
- Gaia Collaboration et al., 2018, *A&A*, **616**, A1
- Gauza B., Béjar V. J. S., Pérez-Garrido A., Rosa Zapatero Osorio M., Lodieu N., Rebolo R., Pallé E., Nowak G., 2015, *ApJ*, **804**, 96
- Geballe T. R., et al., 2002, *ApJ*, **564**, 466
- Gorlova N. I., Meyer M. R., Rieke G. H., Liebert J., 2003, *ApJ*, **593**, 1074
- Greenfield P., White R. L., 2006, in Koekemoer A. M., Goudfrooij P., Dressel L. L., eds, *The 2005 HST Calibration Workshop: Hubble After the Transition to Two-Gyro Mode*. p. 437
- Haisch Jr. K. E., Barsony M., Tinney C., 2010, *ApJL*, **719**, L90
- Hambly N. C., et al., 2008, *MNRAS*, **384**, 637
- Hewett P. C., Warren S. J., Leggett S. K., Hodgkin S. T., 2006, *MNRAS*, **367**, 454
- Hodgkin S. T., Irwin M. J., Hewett P. C., Warren S. J., 2009, *MNRAS*, **394**, 675
- Irwin M. J., et al., 2004, in Quinn P. J., Bridger A., eds, *Optimizing Scientific Return for Astronomy through Information Technologies*. Edited by Quinn, Peter J.; Bridger, Alan. *Proceedings of the SPIE*, Volume 5493, pp. 411–422 (2004).. pp 411–422, doi:10.1117/12.551449
- Iye M., et al., 2004, *PASJ*, **56**, 381
- Jenness T., LSST Data Management Team 2017, in Lorente N. P. F., Shortridge K., Wayth R., eds, *Astronomical Society of the Pacific Conference Series* Vol. 512, *Astronomical Data Analysis Software and Systems XXV*. p. 297 (arXiv:1511.06790)
- Kausch W., et al., 2015, *A&A*, **576**, A78
- Kawanomoto S., et al., 2018, *PASJ*, **70**, 66
- Kirkpatrick J. D., 2005, *ARA&A*, **43**, 195
- Kirkpatrick J. D., et al., 2019, *ApJS*, **240**, 19
- Komiyama Y., et al., 2018, *PASJ*, **70**, S2
- Kratter K. M., Murray-Clay R. A., Youdin A. N., 2010, *ApJ*, **710**, 1375
- Kraus A. L., Ireland M. J., Martinache F., Lloyd J. P., 2008, *ApJ*, **679**, 762
- Kraus A. L., Cody A. M., Covey K. R., Rizzuto A. C., Mann A. W., Ireland M. J., 2015, *ApJ*, **807**, 3
- Kunkel M., 1999, Ph.D. Thesis, Julius-Maximilians-Universität Würzburg, Lafrenière D., Jayawardhana R., van Kerkwijk M. H., 2010, *ApJ*, **719**, 497
- Lafrenière D., Jayawardhana R., Janson M., Helling C., Witte S., Hauschildt P., 2011, *ApJ*, **730**, 42
- Lafrenière D., Jayawardhana R., van Kerkwijk M. H., Brandeker A., Janson M., 2014, *ApJ*, **785**, 47
- Lawrence A., Warren S. J., Almaini O., Edge A. C., Hambly N. C., 17 co-authors 2007, *MNRAS*, **379**, 1599
- Leggett S. K., et al., 2000, *ApJL*, **536**, L35
- Lissauer J. J., Dawson R. I., Tremaine S., 2014, *Nature*, **513**, 336
- Liu M. C., et al., 2013, *ApJL*, **777**, L20
- Liu M. C., Dupuy T. J., Allers K. N., 2016, *ApJ*, **833**, 96
- Lodieu N., 2013, *MNRAS*, **431**, 3222
- Lodieu N., Hambly N. C., Jameson R. F., 2006, *MNRAS*, **373**, 95
- Lodieu N., Hambly N. C., Jameson R. F., Hodgkin S. T., Carraro G., Kendall T. R., 2007a, *MNRAS*, **374**, 372
- Lodieu N., Pinfield D. J., Leggett S. K., Jameson R. F., Mortlock D. J., Warren S. J., co-authors ., 2007b, *MNRAS*, **379**, 1423
- Lodieu N., Hambly N. C., Jameson R. F., Hodgkin S. T., 2008, *MNRAS*, **383**, 1385
- Lodieu N., Hambly N. C., Dobbie P. D., Cross N. J. G., Christensen L., Martin E. L., Valdivielso L., 2011a, *MNRAS*, **418**, 2604
- Lodieu N., Dobbie P. D., Hambly N. C., 2011b, *A&A*, **527**, A24
- Lodieu N., Ivanov V. D., Dobbie P. D., 2013a, *MNRAS*, **430**, 1784
- Lodieu N., Dobbie P. D., Cross N. J. G., Hambly N. C., Read M. A., Blake R. P., Floyd D. J. E., 2013b, *MNRAS*, **435**, 2474
- Lodieu N., et al., 2015, *A&A*, **584**, A128
- Lodieu N., Zapatero Osorio M. R., Béjar V. J. S., Peña Ramírez K., 2018a, *MNRAS*, **473**, 2020
- Lodieu N., Rebolo R., Pérez-Garrido A., 2018b, *A&A*, **615**, L12
- Lodieu N., Paunzen E., Zejda M., 2020, *Low-Mass and Sub-stellar Eclipsing Binaries in Stellar Clusters*. pp 213–243, doi:10.1007/978-3-030-38509-5_8
- Looper D. L., Kirkpatrick J. D., Burgasser A. J., 2007, *AJ*, **134**, 1162
- Low C., Lynden-Bell D., 1976, *MNRAS*, **176**, 367
- Lucas P. W., Roche P. F., 2000, *MNRAS*, **314**, 858
- Luhman K. L., 2012, *ARA&A*, **50**, 65
- Luhman K. L., Esplin T. L., 2020a, *AJ*, **160**, 44
- Luhman K. L., Esplin T. L., 2020b, *AJ*, **160**, 44
- Luhman K. L., Mamajek E. E., 2012, *ApJ*, **758**, 31
- Luhman K. L., Rieke G. H., Lada C. J., Lada E. A., 1998, *ApJ*, **508**, 347
- Luhman K. L., Herrmann K. A., Mamajek E. E., Esplin T. L., Pecaut M. J., 2018, *AJ*, **156**, 76
- Manjavacas E., et al., 2014, *A&A*, **564**, A55
- Mann A. W., et al., 2016, *AJ*, **152**, 61
- Marocco F., et al., 2014, *MNRAS*, **439**, 372
- Martín E. L., Rebolo R., Zapatero Osorio M. R., 1996, *ApJ*, **469**, 706
- Martín E. L., Delfosse X., Guieu S., 2004, *AJ*, **127**, 449
- Mauro F., Moni Bidin C., Chené A.-N., Geisler D., Alonso-García J., Borissova J., Carraro G., 2013, *Revista Mexicana de Astronomía y Astrofísica*, **49**, 189
- Mayor M., Queloz D., 1995, *Nature*, **378**, 355
- McGovern M. R., Kirkpatrick J. D., McLean I. S., Burgasser A. J., Prato L., Lowrance P. J., 2004, *ApJ*, **600**, 1020
- Miller G. E., Scalo J. M., 1979, *ApJS*, **41**, 513
- Miyazaki S., et al., 2018, *PASJ*, **70**, S1
- Mužić K., Scholz A., Geers V. C., Jayawardhana R., López Martí B., 2014, *ApJ*, **785**, 159
- Nakajima T., Oppenheimer B. R., Kulkarni S. R., Golimowski D. A., Matthews K., Durrance S. T., 1995, *Nature*, **378**, 463
- Ochsenbein F., Bauer P., Marcout J., 2000, *A&AS*, **143**, 23
- Peña Ramírez K., Zapatero Osorio M. R., Béjar V. J. S., Rebolo R., Bihain G., 2011, *A&A*, **532**, A42
- Peña Ramírez K., Zapatero Osorio M. R., Béjar V. J. S., 2015, *A&A*, **574**, A118
- Peña Ramírez K., Béjar V. J. S., Zapatero Osorio M. R., 2016, *A&A*, **586**, A157
- Pecaut M. J., Mamajek E. E., Bubar E. J., 2012, *ApJ*, **746**, 154
- Pinfield D. J., Burningham B., Tamura M., Leggett S. K., Lodieu N., Lucas P. W., Mortlock D. J., 28 co-authors 2008, *MNRAS*, **390**, 304
- Preibisch T., Zinnecker H., 1999, *AJ*, **117**, 2381
- Preibisch T., Zinnecker H., 2002, *AJ*, **123**, 1613
- Preibisch T., Guenther E., Zinnecker H., Sterzik M., Frink S., Roeser S., 1998, *A&A*, **333**, 619
- Preibisch T., Guenther E., Zinnecker H., 2001, *AJ*, **121**, 1040
- Rebolo R., Zapatero-Osorio M. R., Martín E. L., 1995, *Nature*, **377**, 129
- Rees M. J., 1976, *MNRAS*, **176**, 483
- Rogers P. D., Wadsley J., 2012, *MNRAS*, **423**, 1896
- Salpeter E. E., 1955, *ApJ*, **121**, 161
- Scalo J. M., 1986, *Fundamentals of Cosmic Physics*, **11**, 1
- Schlafly E. F., Meisner A. M., Green G. M., 2019, *ApJS*, **240**, 30
- Schmidt S. J., West A. A., Hawley S. L., Pineda J. S., 2010, *AJ*, **139**, 1808
- Schneider A. C., Windsor J., Cushing M. C., Kirkpatrick J. D., Wright E. L., 2016, *ApJL*, **822**, L1
- Scholz A., Muzic K., Geers V., Bonavita M., Jayawardhana R., Tamura M., 2012, *ApJ*, **744**, 6
- Science Software Branch at STScI 2012, PyRAF: Python alternative for IRAF, Astrophysics Source Code Library (ascl:1207.011)

- Silk J., 1977, *ApJ*, **214**, 152
- Slesnick C. L., Carpenter J. M., Hillenbrand L. A., 2006, *AJ*, **131**, 3016
- Slesnick C. L., Hillenbrand L. A., Carpenter J. M., 2008, *ApJ*, **688**, 377
- Smette A., et al., 2015, *A&A*, **576**, A77
- Song I., Zuckerman B., Bessell M. S., 2012, *AJ*, **144**, 8
- Spezzi L., Alves de Oliveira C., Moraux E., Bouvier J., Winston E., Hudelot P., Bouy H., Cuillandre J.-C., 2012, *A&A*, **545**, A105
- Stauffer J. R., Schultz G., Kirkpatrick J. D., 1998, *ApJL*, **499**, 199
- Stetson P. B., 1987, *PASP*, **99**, 191
- Tody D., 1986, in Crawford D. L., ed., Society of Photo-Optical Instrumentation Engineers (SPIE) Conference Series Vol. 627, Society of Photo-Optical Instrumentation Engineers (SPIE) Conference Series. p. 733
- Tody D., 1993, in Hanisch R. J., Brissenden R. J. V., Barnes J., eds, Astronomical Society of the Pacific Conference Series Vol. 52, Astronomical Data Analysis Software and Systems II. p. 173
- Vernet J., et al., 2011, *A&A*, **536**, A105
- Walter F. M., Vrba F. J., Mathieu R. D., Brown A., Myers P. C., 1994, *AJ*, **107**, 692
- Whitworth A. P., Stamatellos D., 2006, *A&A*, **458**, 817
- Zapatero Osorio M. R., Béjar V. J. S., Martín E. L., Rebolo R., Barrado y Navascués D., Bailer-Jones C. A. L., Mundt R., 2000, *Science*, **290**, 103
- Zapatero Osorio M. R., Béjar V. J. S., Miles-Páez P. A., Peña Ramírez K., Rebolo R., Pallé E., 2014a, *A&A*, **568**, A6
- Zapatero Osorio M. R., et al., 2014b, *A&A*, **568**, A77
- Zapatero Osorio M. R., et al., 2014c, *A&A*, **572**, A67
- de Bruijne J. H. J., Hoogerwerf R., Brown A. G. A., Aguilar L. A., de Zeeuw P. T., 1997, in ESA SP-402: Hipparcos - Venice '97, pp 575–578
- de Zeeuw P. T., Hoogerwerf R., de Bruijne J. H. J., Brown A. G. A., Blaauw A., 1999, *AJ*, **117**, 354

APPENDIX A: TABLES WITH LIST OF CANDIDATES

This paper has been typeset from a $\text{\TeX}/\text{\LaTeX}$ file prepared by the author.

Table A1. List of USco member candidates that passed our photometric selection criteria ordered by Y magnitude. We list the coordinates in the second epoch deep Y survey (in J2000), optical (deep VISTA Z survey), near-infrared (Y , J from VISTA; H , K from UKIDSS GCS DR9), and mid-infrared ($w1$, $w2$ from ALLWISE) photometry with their error bars and the proper motion in mas/yr of the best photometric candidates. The last part of the table denotes the candidates fainter than the faintest spectroscopic members known in USco newly identified in this work.

ID	R.A.	Dec	Y	J	Z	H	K	$w1$	$w2$	$\mu_{\alpha \cos(\delta)}$	μ_{δ}
	hh:mm:ss.ss	°:':"	mag	mag	mag	mag	mag	mag	mag	mas/yr	mas/yr
53	16:03:50.82	-21:44:56.7	15.015±0.010	14.383±0.018	15.757±0.010	13.820±0.004	—	13.226±0.026	13.029±0.030	-44.7	4.4
48	16:11:17.11	-22:17:17.7	15.103±0.008	14.430±0.009	16.118±0.016	13.768±0.003	13.299±0.003	13.065±0.024	12.742±0.028	-10.0	-19.3
43	16:10:30.14	-23:15:17.1	15.163±0.009	14.382±0.007	16.194±0.007	13.800±0.003	13.266±0.003	13.069±0.025	12.755±0.026	-17.9	-32.3
34	16:10:00.16	-23:12:19.4	15.218±0.009	14.578±0.010	16.093±0.012	13.971±0.004	13.560±0.004	13.391±0.026	13.105±0.031	-38.3	-13.4
41	16:13:30.33	-22:44:06.8	15.255±0.006	14.548±0.010	15.937±0.010	13.965±0.004	13.599±0.004	13.467±0.027	13.265±0.032	-16.6	-13.7
35	16:04:40.25	-22:54:32.6	15.269±0.007	14.481±0.019	16.486±0.013	13.760±0.003	13.268±0.003	12.816±0.025	12.196±0.025	-7.3	-21.6
46	16:13:40.79	-22:19:46.3	15.570±0.006	14.707±0.007	16.580±0.006	14.140±0.004	13.653±0.004	13.416±0.025	13.058±0.030	2.6	-25.7
44	16:10:51.78	-23:33:27.4	15.648±0.007	14.947±0.006	16.460±0.011	14.423±0.005	14.027±0.005	13.819±0.027	13.553±0.039	-56.9	-97.7
50	16:12:53.13	-21:46:27.4	15.688±0.006	14.977±0.020	16.335±0.010	14.553±0.006	14.174±0.006	13.975±0.027	13.788±0.039	-27.0	1.4
32	16:08:30.49	-23:35:11.3	15.753±0.010	14.850±0.006	16.929±0.011	14.311±0.005	13.746±0.005	13.360±0.026	12.841±0.029	-5.4	-17.8
51	16:07:23.81	-22:11:02.2	16.041±0.007	15.133±0.009	17.269±0.013	14.565±0.006	13.989±0.006	13.707±0.027	13.393±0.033	3.5	-29.5
38	16:05:01.90	-23:21:30.5	16.068±0.012	15.148±0.007	17.226±0.010	14.506±0.004	13.968±0.005	13.778±0.028	13.373±0.035	-19.1	-18.4
33	16:09:05.67	-22:45:16.9	16.090±0.006	15.204±0.009	17.321±0.014	14.572±0.006	14.014±0.005	13.817±0.026	13.459±0.033	-3.0	-9.1
55	16:04:42.11	-22:34:11.1	16.228±0.010	15.416±0.012	17.148±0.007	14.812±0.007	14.362±0.007	14.172±0.029	14.013±0.046	-13.1	-65.5
31	16:08:28.46	-23:15:10.6	16.443±0.007	15.490±0.009	17.676±0.008	14.795±0.007	14.138±0.006	13.765±0.027	13.179±0.030	-15.8	-28.0
54	16:06:02.58	-22:02:49.9	16.594±0.007	15.554±0.011	17.916±0.020	14.953±0.007	14.340±0.007	14.097±0.028	13.700±0.041	-33.0	-7.8
56	16:06:03.75	-22:19:30.2	16.914±0.013	15.865±0.015	18.302±0.018	15.112±0.008	14.440±0.007	13.932±0.030	13.307±0.033	-3.7	-16.4
52	16:08:18.42	-22:32:25.2	17.143±0.011	16.140±0.012	18.541±0.012	15.387±0.011	14.676±0.010	14.331±0.031	13.982±0.046	4.1	-7.3
49	16:13:01.39	-21:42:54.8	17.305±0.009	16.390±0.018	18.427±0.010	15.631±0.014	15.070±0.013	14.859±0.035	14.738±0.069	-18.1	-12.7
37	16:04:16.18	-23:26:29.9	17.323±0.013	16.434±0.007	18.685±0.006	15.657±0.012	15.043±0.013	14.669±0.033	14.319±0.056	-49.7	-18.9
47	16:10:38.36	-21:51:47.0	17.464±0.005	16.316±0.020	18.899±0.017	15.473±0.012	14.781±0.009	14.350±0.031	13.807±0.040	-5.6	-30.6
45	16:16:10.64	-21:51:24.5	17.646±0.005	16.555±0.009	18.831±0.008	15.995±0.020	15.451±0.018	—	—	-12.6	-26.7
29	16:07:14.78	-23:21:01.4	17.671±0.008	16.581±0.004	19.124±0.008	15.807±0.016	15.059±0.014	14.464±0.033	13.812±0.041	5.5	-24.1
30	16:07:37.97	-22:42:47.2	17.822±0.011	16.819±0.008	19.412±0.024	16.091±0.020	15.450±0.019	15.098±0.039	14.743±0.075	-1.1	-12.1
36	16:06:09.04	-23:38:11.6	18.033±0.006	16.911±0.008	19.501±0.012	16.247±0.020	15.564±0.020	15.176±0.044	14.895±0.085	-7.2	-13.0
39	16:04:36.56	-23:25:24.1	18.256±0.023	17.145±0.020	19.664±0.018	16.348±0.021	15.671±0.024	—	—	-12.5	-27.8
57	16:05:12.06	-21:45:28.4	18.358±0.010	17.080±0.010	19.792±0.012	16.403±0.024	15.645±0.020	—	—	-11.1	-23.0
40	16:14:20.44	-22:59:52.5	18.463±0.006	17.443±0.013	19.615±0.016	16.753±0.034	16.313±0.044	16.268±0.086	16.585±0.365	-44.6	-59.9
42	16:14:22.56	-23:31:17.9	18.658±0.009	17.442±0.012	20.224±0.023	16.830±0.034	16.080±0.031	—	—	10.3	-20.8
8	16:14:02.87	-23:14:42.7	19.094±0.008	17.879±0.009	20.329±0.012	17.215±0.051	16.606±0.053	16.182±0.074	15.860±0.169	6.2	-7.6
9	16:15:32.35	-22:59:51.0	19.109±0.007	17.878±0.009	20.396±0.020	17.240±0.056	16.564±0.058	15.822±0.055	15.639±0.146	-20.0	29.1
27	16:06:01.43	-22:06:16.3	19.193±0.008	18.037±0.009	20.401±0.032	17.319±0.055	16.792±0.059	16.489±0.092	16.162±0.227	-23.3	10.5
21	16:07:55.40	-22:33:52.5	19.223±0.015	18.055±0.010	20.286±0.028	17.522±0.070	16.860±0.065	—	—	-33.4	4.8
25	16:09:56.36	-22:22:45.9	19.278±0.016	17.871±0.016	20.589±0.016	16.915±0.039	16.221±0.035	—	—	4.5	-37.6
23	16:09:06.61	-21:41:05.3	19.293±0.005	18.128±0.018	20.628±0.021	17.398±0.067	16.758±0.059	16.687±0.106	16.123±0.217	-25.4	-3.0
20	16:07:31.61	-21:46:54.5	19.523±0.009	18.000±0.013	20.938±0.034	17.004±0.046	16.200±0.034	15.147±0.040	14.596±0.062	6.2	-12.5
24	16:09:18.67	-22:29:23.9	19.534±0.017	17.948±0.009	20.786±0.013	16.974±0.041	16.139±0.033	15.539±0.051	15.317±0.114	-33.2	-16.1
4	16:04:13.03	-22:41:03.4	19.553±0.027	18.193±0.020	20.800±0.050	17.235±0.054	16.416±0.042	15.462±0.049	15.254±0.105	-17.0	-7.9
12	16:13:34.65	-21:36:20.3	19.644±0.008	18.207±0.017	20.918±0.017	17.111±0.045	16.385±0.039	15.744±0.053	15.369±0.120	34.4	11.5
14	16:14:07.56	-22:11:52.3	19.705±0.009	18.224±0.016	21.105±0.020	17.386±0.070	16.384±0.049	15.570±0.051	15.290±0.105	3.4	-23.0
17	16:11:10.15	-21:45:16.9	19.745±0.017	18.410±0.027	21.938±0.144	17.303±0.057	16.441±0.040	—	—	-0.6	-30.4
19	16:11:44.37	-22:15:44.7	19.822±0.008	17.909±0.010	20.730±0.027	16.871±0.044	15.898±0.030	15.303±0.045	14.726±0.070	-1.3	-16.9
3	16:08:43.43	-22:45:16.2	19.850±0.018	18.317±0.021	21.162±0.041	17.192±0.056	16.299±0.040	15.412±0.045	14.670±0.069	-4.8	-6.0
28	16:04:20.42	-21:34:53.1	19.899±0.012	18.448±0.012	21.113±0.022	17.432±0.061	16.498±0.045	15.695±0.051	15.332±0.110	-27.4	-14.5
26	16:08:42.37	-22:23:26.3	19.909±0.012	18.625±0.020	21.169±0.025	17.870±0.094	17.245±0.091	16.959±0.149	16.118±0.235	-8.4	-60.5
18	16:11:10.83	-22:03:47.6	20.081±0.011	18.857±0.012	21.260±0.027	18.047±0.118	17.325±0.092	—	—	16.4	-23.3
16	16:11:05.28	-22:22:57.4	20.466±0.016	19.149±0.019	21.953±0.046	18.461±0.192	17.313±0.109	—	—	-8.3	-11.5
5	16:04:31.51	-23:13:04.4	20.549±0.013	19.123±0.021	21.905±0.046	18.464±0.152	17.629±0.140	—	—	-31.9	6.9
13	16:15:15.22	-21:48:46.6	20.922±0.015	19.515±0.029	22.287±0.051	—	—	—	—	21.7	-7.0
15	16:15:12.70	-22:29:49.2	20.943±0.019	19.264±0.025	22.307±0.071	18.167±0.142	17.065±0.087	16.529±0.100	15.729±0.156	-7.9	1.4
22	16:08:34.28	-21:48:04.9	20.984±0.015	19.346±0.039	22.269±0.094	—	17.799±0.152	17.022±0.153	16.939±0.476	-10.0	3.0
11	16:12:37.84	-22:51:12.9	21.781±0.038	19.504±0.039	22.259±0.062	—	—	—	—	83.9	-564.2
6	16:05:17.84	-23:35:51.9	21.824±0.019	18.064±0.029	21.960±0.055	—	—	—	—	-259.8	-17.4
1	16:09:29.08	-23:40:48.2	21.909±0.136	19.336±0.040	22.700±0.083	18.368±0.168	—	—	—	-486.5	-47.5
7	16:04:04.50	-23:21:31.0	22.164±0.049	19.688±0.050	22.496±0.082	—	—	—	—	-155.2	-350.4
10	16:15:04.04	-22:40:13.3	22.199±0.097	19.556±0.022	22.634±0.084	18.430±0.170	—	—	—	377.2	-356.6
2	16:10:03.24	-23:18:11.8	22.756±0.078	20.444±0.068	23.296±0.159	—	—	17.500±0.199	16.519±0.000	-564.3	-43.1

Table A2. List of USco member YJ candidates undetected in the deep VISTA Z -band survey. They are among the 10 newly identified potential candidates fainter than the coolest members known in USco. None of these candidates has counterparts in UKIDSS GCS DR9, AllWISE, and PanStarrs. Only the last object in the table has a Z magnitude from the deep Subaru/HSC survey ($Z = 22.959 \pm 0.025$ mag; Table A3). We give their ID number, coordinates in the second epoch deep Y survey (in J2000), YJ photometry with their error bars, and the proper motion in mas/yr measured between the first (J) and second (Y) epoch VISTA surveys.

ID	R.A.	Dec	Y	J	$\mu_{\alpha} \cos \delta$	μ_{δ}
	hh:mm:ss.ss	°:′:″	mag	mag	mas/yr	mas/yr
candYJ_VISTA_101	16:09:13.79	-23:35:46.9	22.227±0.166	20.247±0.089	-149.5	109.0
candYJ_VISTA_102	16:04:46.67	-22:52:41.4	22.459±0.085	20.367±0.083	-272.8	65.1
candYJ_VISTA_103	16:06:26.99	-22:50:00.6	22.183±0.129	20.086±0.058	-352.1	448.9
candYJ_VISTA_104	16:14:41.41	-22:16:29.8	22.669±0.070	19.569±0.046	-330.8	340.0

Table A3. List of USco member YJ candidates with detections in the Subaru/HSC Z -band survey. We give their ID number, coordinates in the second epoch deep Y survey (in J2000), Subaru Z photometry, YJ photometry with their error bars. The two brightest in Z appear as the best candidates because they extend the USco sequence shown in colour-colour diagrams involving the ZYJ filters.

ID	R.A.	Dec	Z	Y	J
	hh:mm:ss.ss	°:′:″	mag	mag	mag
candYJ_HSC_1005	16:12:03.71	-22:35:09.4	23.879±0.064	22.318±0.077	20.536±0.081
candYJ_HSC_1002	16:13:59.13	-22:12:36.8	24.192±0.100	23.082±0.122	21.176±0.114
candYJ_HSC_1001	16:14:14.47	-23:12:36.7	24.266±0.096	22.961±0.171	21.082±0.107
candYJ_HSC_1003	16:14:41.41	-22:16:29.8	22.959±0.025	22.669±0.070	19.569±0.046
candYJ_HSC_1004	16:15:32.45	-22:11:05.4	23.994±0.073	22.964±0.126	21.202±0.126